Published for SISSA by Springer

Received: *March 14, 2018*
Revised: *June 13, 2018*
Accepted: *July 15, 2018*
Published: *August 13, 2018*

Evidence for associated production of a Higgs boson with a top quark pair in final states with electrons, muons, and hadronically decaying τ leptons at $\sqrt{s} = 13$ TeV

The CMS collaboration

E-mail: cms-publication-committee-chair@cern.ch

Abstract: Results of a search for the standard model Higgs boson produced in association with a top quark pair ($t\bar{t}H$) in final states with electrons, muons, and hadronically decaying τ leptons are presented. The analyzed data set corresponds to an integrated luminosity of 35.9 fb^{-1} recorded in proton-proton collisions at $\sqrt{s} = 13$ TeV by the CMS experiment in 2016. The sensitivity of the search is improved by using matrix element and machine learning methods to separate the signal from backgrounds. The measured signal rate amounts to $1.23^{+0.45}_{-0.43}$ times the production rate expected in the standard model, with an observed (expected) significance of 3.2σ (2.8σ), which represents evidence for $t\bar{t}H$ production in those final states. An upper limit on the signal rate of 2.1 times the standard model production rate is set at 95% confidence level.

Keywords: Hadron-Hadron scattering (experiments), Higgs physics, Top physics

ArXiv ePrint: 1803.05485

https://doi.org/10.1007/JHEP08(2018)066

JHEP08(2018)066

Contents

1 Introduction

The observation of a Higgs boson (H) by the ATLAS and the CMS experiments [1–3] represents a major step towards the understanding of the mechanism for electroweak symmetry breaking (EWSB). The current most precise measurement of the Higgs boson mass, obtained by the CMS Collaboration, is 125.26±0.21 GeV [4]. The standard model (SM) makes

JHEP08(2018)066

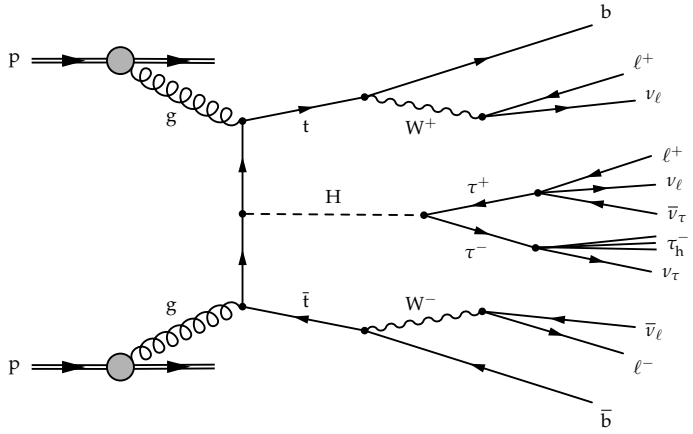

Figure 1. An example of a Feynman diagram for $t\bar{t}H$ production, with subsequent decay of the Higgs boson to a pair of τ leptons, producing a final state with two same-sign leptons and one reconstructed hadronic τ lepton decay (τ_h).

precise predictions for all properties of the Higgs boson, given its mass. Within uncertainties, all measured properties of the discovered resonance are consistent with expectations for the SM Higgs boson, corroborating the mechanism for EWSB in the SM. In particular, the discovered particle is known to have zero spin and positive parity [5, 6]. Within the present experimental uncertainties, its coupling to fermions is found to be proportional to the fermion mass, as predicted by the SM. In order to confirm that the mechanism for EWSB included in the SM is indeed realized in nature, it is important to perform more precise measurements of the Higgs boson properties.

The measurement of the Yukawa coupling of the Higgs boson to the top quark, y_t, is of high phenomenological interest for several reasons. The extraordinarily large value of the top quark mass, compared to the masses of all other known fermions, may indicate that the top quark plays a still-unknown special role in the EWSB mechanism. The measurement of the rate at which Higgs bosons are produced in association with top quark pairs ($t\bar{t}H$ production) provides the most precise model-independent determination of y_t. An example of a Feynman diagram for $t\bar{t}H$ production in proton-proton (pp) collisions is shown in figure 1. Since the rate for the gluon fusion Higgs boson production process is dominated by top quark loops, a comparison of y_t measured through this production channel and through the $t\bar{t}H$ production channel will provide powerful constraints on new physics potentially introduced into the gluon fusion process by additional loop contributions.

The associated production of a Higgs boson with a top quark pair in pp collisions at a center-of-mass energy of $\sqrt{s} = 8\,\text{TeV}$ has been studied in the $H \to bb$ and $H \to \gamma\gamma$ decay modes as well as in multilepton final states by the ATLAS and CMS Collaborations [7–12]. The final states with multiple leptons cover the decay modes $H \to WW$, $H \to ZZ$, and $H \to \tau\tau$. The ATLAS Collaboration recently reported evidence for the $t\bar{t}H$ process observed in the combination of several final states with data recorded at $\sqrt{s} = 13\,\text{TeV}$ [13, 14]. In this paper, we present the results of a search for $t\bar{t}H$ production in multilepton final states in pp collision data recorded with the CMS detector at $\sqrt{s} = 13\,\text{TeV}$. The analysis is performed

JHEP08(2018)066

in six event categories, distinguished by the number of light charged leptons (electrons and muons, generically referred to as leptons in the rest of this document) and the number of reconstructed hadronic τ lepton decays in the event. We denote by the symbol τ_h the system of charged and neutral hadrons produced in hadronic τ lepton decays. The sensitivity of the analysis is enhanced by means of multivariate analysis (MVA) techniques based on boosted decision trees (BDTs) [15, 16] and by matrix element method (MEM) discriminants [17, 18].

This paper is structured as follows: the apparatus and the data samples are described in sections 2 and 3. Section 4 summarizes the event reconstruction. The event selection and the background estimation are described in sections 5 and 6. Section 7 focuses on the signal extraction techniques. The systematic uncertainties are discussed in section 8. Section 9 presents event yields, kinematic distributions, and measured properties, while the results are summarized in section 10. Details about the MEM computation are provided in appendix A.

2 The CMS detector

The central feature of the CMS apparatus is a superconducting solenoid of 6 m internal diameter, providing a magnetic field of 3.8 T. A silicon pixel and strip tracker, a lead tungstate crystal electromagnetic calorimeter (ECAL), and a brass and scintillator hadron calorimeter (HCAL), each composed of a barrel and two endcap sections, are positioned within the solenoid volume. The silicon tracker measures charged particles within the pseudorapidity range $|\eta| < 2.5$. Tracks of isolated muons of transverse momentum $p_T \geq 100$ GeV emitted at $|\eta| < 1.4$ are reconstructed with an efficiency close to 100% and resolutions of 2.8% in p_T and 10 (30) μm in the transverse (longitudinal) impact parameter [19]. The ECAL is a fine-grained hermetic calorimeter with quasi-projective geometry, and is segmented into the barrel region of $|\eta| < 1.48$ and in two endcaps that extend up to $|\eta| < 3.0$. The HCAL barrel and endcaps similarly cover the region $|\eta| < 3.0$. Forward calorimeters extend the coverage up to $|\eta| < 5.0$. Muons are measured and identified in the range $|\eta| < 2.4$ by gas-ionization detectors embedded in the steel flux-return yoke outside the solenoid. A two-level trigger system is used to reduce the rate of recorded events to a level suitable for data acquisition and storage [20]. The first level of the CMS trigger system, composed of custom hardware processors, uses information from the calorimeters and muon detectors to select the most interesting events in a fixed time interval of less than 4 μs. The high-level trigger processor farm further decreases the event rate from around 100 kHz to less than 1 kHz. Details of the CMS detector and its performance, together with a definition of the coordinate system and the kinematic variables used in the analysis, can be found in ref. [21].

3 Data samples and Monte Carlo simulation

The analyzed data set was collected in pp collisions at $\sqrt{s} = 13$ TeV in 2016 and corresponds to an integrated luminosity of 35.9 fb^{-1}. The events were recorded using a combination of

JHEP08(2018)066

triggers based on the presence of one, two, or three electrons and muons or based on the presence of an electron or muon and a hadronic τ lepton decay.

The data are compared to signal and background estimations based on Monte Carlo (MC) simulated samples and data-driven techniques. The main irreducible background to the analysis, arising from the associated production of a top quark pair with one or two W or Z bosons ($\mathrm{t\bar{t}Z}$, $\mathrm{t\bar{t}W}$, and $\mathrm{t\bar{t}WW}$) is modeled using MC simulation. The sum of these contributions is referred to as the $\mathrm{t\bar{t}V}$ background. Other relevant backgrounds that are modeled by MC simulation include $\mathrm{Z}\gamma$+jets, $\mathrm{W}\gamma$+jets, $\mathrm{t\bar{t}}\gamma$ and $\mathrm{t\bar{t}}\gamma^*$, single top, diboson (WW, WZ, and ZZ) and triboson (WWW, WWZ, WZZ, and ZZZ) production, the production of SM Higgs bosons in association with single top quarks (tH), and a few selected "rare" processes. These rare processes, such as $\mathrm{t\bar{t}t\bar{t}}$, and the production of same-sign W boson pairs, typically have very small cross sections, but may nevertheless yield nonnegligible background contributions. The contribution to the signal regions from the production of SM Higgs bosons through the gluon fusion and vector boson fusion processes, as well as their production in association with W or Z bosons, is negligible. Separate event samples are generated to simulate the production of single top quarks in association with jets, photons, and W and Z bosons. The reducible Z+jets, W+jets and $\mathrm{t\bar{t}}$+jets backgrounds are determined from data. Simulated $\mathrm{t\bar{t}}$+jets samples, produced using the leading order (LO) matrix elements implemented in the MadGraph5_aMC@NLO 2.2.2 program [22–24], are used solely for the purpose of validating the data-driven background estimation methods. Samples for other background processes and for the $\mathrm{t\bar{t}H}$ signal are generated using next-to-leading order (NLO) matrix elements implemented in the programs MadGraph5_aMC@NLO and powheg $v2$ [25–28]. The signal events are generated for a Higgs boson mass of $M_{\mathrm{H}} = 125\,\mathrm{GeV}$, while a top quark mass of $M_{\mathrm{t}} = 172.5\,\mathrm{GeV}$ is used for all simulated processes involving a top quark. All samples are generated using the NNPDF3.0 [29–31] set of parton distribution functions (PDFs). Parton shower and hadronization processes are modeled using the generator pythia 8.212 [32] with the CUETP8M1 tune [33]. The decays of τ leptons, including polarization effects, are modeled by pythia. All samples containing top quark pairs as well as the $\mathrm{Z}/\gamma^* \to \ell\ell$ and W+jets samples are normalized to cross sections computed at next-to-next-to-leading order accuracy in perturbative quantum chromodynamics (pQCD) [34, 35]. The cross sections for single top quark [36–38] and diboson [39] production are computed at NLO accuracy in pQCD.

Minimum bias events generated with pythia are overlaid on all simulated events according to the luminosity profile of the analyzed data. In the analyzed data set, an average of approximately 23 inelastic pp interactions (pileup) occur per bunch crossing.

All generated events are passed through a detailed simulation of the CMS apparatus, based on Geant4 [40], and are processed using the same version of the CMS event reconstruction software as used for data.

Small corrections are applied to simulated events as data-to-MC scale factors in order to improve the modeling of the data. The efficiency of the triggers based on the presence of one, two, or three electrons or muons, as well as the efficiency for electrons or muons to pass the lepton reconstruction, identification, and isolation criteria, are measured using

JHEP08(2018)066

$Z/\gamma^* \to ee$ and $Z/\gamma^* \to \mu\mu$ events. The efficiency of the triggers based on the presence of an electron or muon and a hadronic τ lepton decay, the efficiency for hadronic τ lepton decays to pass the τ_h identification criteria, and the energy scale with which hadronic τ lepton decays are reconstructed, are measured using $Z/\gamma^* \to \tau\tau$ events [41]. The b tagging efficiency and mistag rate (discussed in section 4.4) are measured in $t\bar{t}$+jets and $Z/\gamma^* \to \ell\ell$ events [42], respectively. The differences in the resolution of the missing transverse momentum between data and simulation are measured in $Z/\gamma^* \to \ell\ell$ and γ+jets events [43] and corrected as described in ref. [44].

4 Event reconstruction

The information provided by all CMS subdetectors is employed by a particle-flow (PF) algorithm [45] to identify and reconstruct individual particles in the event, namely muons, electrons, photons, and charged and neutral hadrons. These particles are then used to reconstruct jets, τ_h and the vector p_T imbalance in the event, referred to as $\vec{p}_T^{\,miss}$, as well as to quantify the isolation of leptons.

4.1 Vertices

Collision vertices are reconstructed using a deterministic annealing algorithm [46, 47]. The reconstructed vertex position is required to be compatible with the location of the LHC beam in the x–y plane. The reconstructed vertex with the largest value of summed physics-object p_T^2 is taken to be the primary pp interaction vertex (PV). The physics objects are the jets, clustered using the jet finding algorithm [48, 49] with the tracks assigned to the vertex as inputs, and the associated missing transverse momentum, taken as the negative vector sum of the p_T of those jets. Electrons, muons, and τ_h candidates, which are subsequently reconstructed, are required to be compatible with originating from the selected PV.

4.2 Electrons and muons

Electrons are reconstructed within $|\eta| < 2.5$ by an algorithm [50] that matches tracks reconstructed in the silicon tracker to energy deposits in the ECAL, without any significant energy deposit in the HCAL. Tracks of electron candidates are reconstructed by a dedicated algorithm which accounts for the emission of bremsstrahlung photons. The energy loss due to bremsstrahlung is determined by searching for energy deposits in the ECAL located tangentially to the track. An MVA approach based on BDTs is employed to distinguish electrons from hadrons mimicking an electron signature. Observables that quantify the quality of the electron track, the compactness of the electron cluster, and the matching between the track momentum and direction with the sum and position of energy deposits in the ECAL are used as inputs to the BDT. This electron identification BDT has been trained on samples of electrons and hadrons. Additional requirements are applied in order to remove electrons originating from photon conversions [50].

The identification of muons is based on linking track segments reconstructed in the silicon tracking detector and in the muon system [51] within $|\eta| < 2.4$. The matching between track segments is done outside-in, starting from a track in the muon system,

JHEP08(2018)066

and inside-out, starting from a track reconstructed in the inner detector. If a link can be established, the track parameters are recomputed using the combination of hits in the inner and outer detectors. Quality requirements are applied on the multiplicity of hits in the track segments, on the number of matched track segments and on the quality of the track fit [51].

Electrons and muons in signal events are expected to be isolated, while leptons from charm (c) and bottom (b) quark decays as well as from in-flight decays of pions and kaons are often reconstructed near jets. Isolated leptons are distinguished from nonisolated leptons using the scalar p_{T} sum over charged particles, neutral hadrons, and photons that are reconstructed within a narrow cone centered on the lepton direction. The size R of the cone shrinks with the increasing p_{T} of the lepton in order to increase the efficiency for leptons reconstructed in signal events with high hadronic activity to pass the isolation criteria. The narrow cone size, referred to as "mini-isolation", has the further advantage that it reduces the effect of pileup. Efficiency loss due to pileup is additionally reduced by considering only those charged particles that originate from the lepton production vertex in the isolation sum. Residual contributions of pileup to the neutral component of the isolation I_ℓ of the lepton are taken into account by means of so-called effective area corrections:

$$I_\ell = \sum_{\text{charged}} p_{\mathrm{T}} + \max\left(0, \sum_{\text{neutrals}} p_{\mathrm{T}} - \rho\,\mathcal{A}\left[\frac{R}{0.3}\right]^2\right), \tag{4.1}$$

where ρ represents the energy density of neutral particles reconstructed within the geometric acceptance of the tracking detectors, computed as described in refs. [52, 53]. The effective area $\mathcal{A}$ is obtained from the simulation, by studying the correlation between I_ℓ and ρ, and is determined separately for electrons and muons and in bins of η. The size of the cone is given by:

$$R = \begin{cases} 0.05, & \text{if} \quad p_{\mathrm{T}} > 200\,\text{GeV} \\ 10\,\text{GeV}/p_{\mathrm{T}}, & \text{if} \quad 50 < p_{\mathrm{T}} < 200\,\text{GeV} \\ 0.20, & \text{if} \quad p_{\mathrm{T}} < 50\,\text{GeV} \end{cases}. \tag{4.2}$$

Additional selection criteria are applied to discriminate leptons produced in the decays of W bosons, Z bosons, or τ leptons from those produced in the decays of B or light mesons. We will refer to the former as "prompt" (signal) leptons and to the latter as "nonprompt" (background) leptons. The separation of prompt from nonprompt leptons is performed by a BDT-based algorithm, referred to as the lepton MVA. The following observables are used as input to the lepton MVA: the isolation of the lepton with respect to charged and neutral particles, corrected for pileup effects; the ratio of the p_{T} of the lepton to the p_{T} of the nearest jet; a discriminant that quantifies the probability of this jet to originate from the hadronization of a c or b quark (described in section 4.4); the component of the lepton momentum perpendicular to the jet axis; the transverse and longitudinal impact parameters of the lepton track with respect to the PV; and the significance of the impact parameter, given by the impact parameter (in three dimensions) divided by its uncertainty, of the lepton track with respect to the PV. The last three inputs are the p_{T} and η of the lepton

JHEP08(2018)066

and an additional observable, which improves the discrimination of prompt leptons from residual backgrounds in which the reconstructed lepton arises from the misidentification of a light-quark or gluon jet. For electrons, this additional observable is the output of the MVA that is used for electron identification. For muons, it corresponds to the compatibility of track segments in the muon system with the pattern expected from muon ionization. Inputs that require the matching of the lepton to a nearby jet are set to zero if no jet of $p_{\mathrm{T}} > 10\,\mathrm{GeV}$ is reconstructed within a distance $\Delta R = \sqrt{(\eta_{\mathrm{j}} - \eta_{\ell})^2 + (\phi_{\mathrm{j}} - \phi_{\ell})^2} < 0.4$ from the lepton, where ϕ is the azimuthal angle in radians. Separate lepton MVAs are trained for electrons and muons, using simulated samples of prompt leptons in $\mathrm{t\bar{t}H}$ signal events and nonprompt leptons in $\mathrm{t\bar{t}}$+jets background events. Leptons selected in the signal region are required to pass a tight selection on the lepton MVA output. Looser selection criteria for electrons and muons, referred to as the "relaxed lepton selection", are defined by relaxing the lepton MVA selection for the purpose of estimating the contribution of background processes as detailed in section 6.

4.3 Hadronic τ lepton decays

Hadronic τ lepton decays are reconstructed by the "hadrons-plus-strips" (HPS) algorithm [54] within $|\eta| < 2.3$. The algorithm reconstructs individual hadronic decay modes of the τ lepton: $\tau^{\pm} \to \mathrm{h}^{\pm}\nu_{\tau}$, $\tau^{\pm} \to \mathrm{h}^{\pm}\pi^0\nu_{\tau}$, $\tau^{\pm} \to \mathrm{h}^{\pm}\pi^0\pi^0\nu_{\tau}$, and $\tau^{\pm} \to \mathrm{h}^{\pm}\mathrm{h}^{\mp}\mathrm{h}^{\pm}\nu_{\tau}$, where $\mathrm{h}^{\pm}$ denotes either a charged pion or kaon. Hadronic τ candidates are built by combining the charged hadrons reconstructed by the PF algorithm with neutral pions. The neutral pions are reconstructed by clustering the photons and electrons reconstructed by the PF algorithm within rectangular strips that are narrow in η, but wide in the ϕ direction, to account for the broadening of energy deposits in the ECAL if one of the photons produced in $\pi^0 \to \gamma\gamma$ decays converts within the tracking detector. An improved version of the strip reconstruction has been developed for data analyses at 13 TeV and beyond, replacing the one used in CMS analyses at $\sqrt{s} = 7$ and 8 TeV that was based on a fixed strip size of 0.05×0.20 in η–ϕ. In the improved version the size of the strip is adjusted as a function of the p_{T} of the particles reconstructed within the strip [41].

Tight isolation requirements provide the most effective way to distinguish hadronic τ lepton decays from a large background of light-quark and gluon jets. The sums of scalar p_{T} values of charged particles and of photons are used as inputs to a BDT-based τ_{h} identification discriminant. Separate sums are used for charged particles that are compatible with originating from the τ_{h} production vertex and those that are not. The final additions to the list of input variables are the reconstructed τ_{h} decay mode and observables that provide sensitivity to the lifetime of the τ lepton. The transverse impact parameter of the highest p_{T} track of the τ_{h} candidate with respect to the PV is used for τ_{h} candidates reconstructed in any decay mode. In case of τ_{h} candidates reconstructed in the decay mode $\tau^- \to \mathrm{h}^-\mathrm{h}^+\mathrm{h}^-\nu_{\tau}$, a fit of the three tracks to a common secondary vertex is attempted and the distance to the PV is used as an additional input variable to the BDT. The isolation is computed within a cone of size $R = 0.3$, centered on the τ_{h} direction. Compared to the version of the HPS algorithm used by the majority of CMS analyses with hadronic τ lepton decays, which use a cone of size $R = 0.5$, the size of the cone is reduced in this analysis in

JHEP08(2018)066

order to improve the efficiency in signal events with high hadronic activity. The BDT has been trained on samples of hadronic τ lepton decays in $\mathrm{t\bar{t}H}$ signal events and jets in $\mathrm{t\bar{t}}$+jets background events, produced using MC simulation [41]. Loose, medium, and tight working points (WPs), corresponding respectively to a 65, 55 and 45% τ_h identification efficiency and a 2, 1 and 0.5% jet $\to \tau_\mathrm{h}$ misidentification rate, are defined by varying the selections on the BDT output. The selections are adjusted as a function of the p_T of the τ_h candidate such that the τ_h identification efficiency for each WP is constant as a function of p_T. The loose WP is used for the estimation of the background due to the misreconstruction of light-quark or gluon jets as τ_h candidates and is referred to as the "relaxed τ_h selection". Contamination from events where the reconstructed τ_h originates from a misreconstructed muon or electron is reduced by requiring the reconstructed τ_h not to overlap with muons or electrons passing loose selection criteria within $\Delta R < 0.3$.

4.4 Jets

Jets are reconstructed from the PF candidates using the anti-k_T algorithm [48, 49] with a distance parameter of 0.4, and with the constraint that the charged particles are compatible with the selected PV. Reconstructed jets are required not to overlap with identified electrons, muons or τ_h within $\Delta R < 0.4$ and to pass identification criteria that aim to reject spurious jets arising from calorimeter noise [55]. The energy of reconstructed jets is calibrated as a function of jet p_T and η [56]. Jet energy corrections based on the FastJet algorithm [52, 53] are applied. Jets selected for this analysis must have a $p_\mathrm{T} > 25\,\mathrm{GeV}$ and $|\eta| < 2.4$. Jets originating from the hadronization of b quarks are identified by the "combined secondary vertex" algorithm [42, 57], which exploits observables related to the long lifetime of b hadrons and to the higher particle multiplicity and mass of b jets compared to light-quark and gluon jets. Loose and tight b tagging criteria WPs are used, respectively associated with a mistag rate of 10 and 1% and yielding a b jet selection efficiency of 85 and 70%.

4.5 Missing transverse momentum

The $\vec{p}_\mathrm{T}^{\,\mathrm{miss}}$ is calculated as the negative of the vector p_T sum of all particles reconstructed by the PF algorithm. The magnitude of the vector is referred to as $p_\mathrm{T}^\mathrm{miss}$. The $p_\mathrm{T}^\mathrm{miss}$ resolution and response are improved by propagating the difference between calibrated and uncalibrated jets to the $p_\mathrm{T}^\mathrm{miss}$ and by applying corrections that account for pileup effects, as described in ref. [44].

The $p_\mathrm{T}^\mathrm{miss}$ is complemented by the observable $H_\mathrm{T}^\mathrm{miss}$, defined as the magnitude of the vectorial p_T sum of leptons, τ_h, and jets:

$$H_\mathrm{T}^\mathrm{miss} = \left| \sum_\mathrm{leptons} \vec{p}_{\mathrm{T}\ell} + \sum_{\tau_\mathrm{h}} \vec{p}_{\mathrm{T}\tau} + \sum_\mathrm{jets} \vec{p}_\mathrm{Tj} \right|. \tag{4.3}$$

Leptons and τ_h entering the sum are required to pass the relaxed selection criteria discussed in sections 4.2 and 4.3, while the jets are required to satisfy $p_\mathrm{T} > 25\,\mathrm{GeV}$ and $|\eta| < 2.4$. The resolution on $H_\mathrm{T}^\mathrm{miss}$ is worse compared to the resolution on $p_\mathrm{T}^\mathrm{miss}$. The advantage of

JHEP08(2018)066

the observable $H_{\mathrm{T}}^{\mathrm{miss}}$ is that leptons, τ_{h}, and high p_{T} jets predominantly originate from the hard scattering interaction and rarely from pileup interactions, which makes $H_{\mathrm{T}}^{\mathrm{miss}}$ less sensitive to variations in pileup conditions.

The two observables $p_{\mathrm{T}}^{\mathrm{miss}}$ and $H_{\mathrm{T}}^{\mathrm{miss}}$ are combined into a single linear discriminant:

$$L_{\mathrm{D}} = 0.6\, p_{\mathrm{T}}^{\mathrm{miss}} + 0.4\, H_{\mathrm{T}}^{\mathrm{miss}}, \tag{4.4}$$

exploiting the fact that $p_{\mathrm{T}}^{\mathrm{miss}}$ and $H_{\mathrm{T}}^{\mathrm{miss}}$ are less correlated in events in which the reconstructed $p_{\mathrm{T}}^{\mathrm{miss}}$ is due to instrumental effects compared to events with genuine $p_{\mathrm{T}}^{\mathrm{miss}}$ that arises from the presence of neutrinos. The coefficients of the linear combination have been optimized to provide the best rejection against the Z+jets background.

5 Event selection

This analysis focuses on final states in which one lepton is produced in one of the top quark decays, while the additional leptons and τ_{h} are produced in the Higgs boson or the other top quark decay. The analysis is performed using six mutually exclusive event categories, based on the number of reconstructed leptons and τ_{h} candidates:

- one lepton and two τ_{h} ($1\ell + 2\tau_{\mathrm{h}}$),
- two leptons with same sign of the charge ("same-sign leptons") and zero τ_{h} ($2\ell\mathrm{ss}$),
- two same-sign leptons and one τ_{h} ($2\ell\mathrm{ss} + 1\tau_{\mathrm{h}}$),
- three leptons and zero τ_{h} (3ℓ),
- three leptons and one τ_{h} ($3\ell + 1\tau_{\mathrm{h}}$), and
- four leptons (4ℓ).

The categories with no τ_{h} are mostly sensitive to the Higgs boson decay into W or Z bosons while the categories with at least one τ_{h} enhance the sensitivity to the Higgs boson decay into τ leptons. The targeted $\mathrm{t\bar{t}H}$ decays in each category are highlighted in tables 1 and 2.

Events in the $2\ell\mathrm{ss}$ and $2\ell\mathrm{ss} + 1\tau_{\mathrm{h}}$ categories are recorded by a combination of single-lepton triggers and triggers that select events containing lepton pairs. In the $1\ell + 2\tau_{\mathrm{h}}$ category, the single-lepton triggers are complemented by triggers that select events containing an electron or muon in combination with a τ_{h}. The efficiency to select signal events in 3ℓ, $3\ell + 1\tau_{\mathrm{h}}$, and 4ℓ categories is increased by collecting events using a combination of single-lepton and dilepton triggers, and triggers based on the presence of three leptons.

The p_{T} thresholds applied in order to select the leptons in different event categories are dictated by trigger requirements. In the $2\ell\mathrm{ss}$, 3ℓ, and 4ℓ categories, the lepton of highest p_{T} ("leading" lepton) is required to satisfy the condition $p_{\mathrm{T}} > 25\,\mathrm{GeV}$ and the lepton of second-highest p_{T} ("subleading" lepton) is required to satisfy $p_{\mathrm{T}} > 15\,\mathrm{GeV}$. The third (fourth) lepton is required to have $p_{\mathrm{T}} > 15(10)\,\mathrm{GeV}$. In the $1\ell + 2\tau_{\mathrm{h}}$ category, the leading lepton is required to pass a threshold of $p_{\mathrm{T}} > 25(20)\,\mathrm{GeV}$ if it is an electron (or muon) and

JHEP08(2018)066

Selection	2ℓss	$2\ell\text{ss} + 1\tau_\text{h}$
Targeted $\text{t}\bar{\text{t}}\text{H}$ decay	$\text{t} \to \text{b}\ell\nu$, $\text{t} \to \text{bqq}$, $\text{H} \to \text{WW} \to \ell\nu\text{qq}$	$\text{t} \to \text{b}\ell\nu$, $\text{t} \to \text{bqq}$, $\text{H} \to \tau\tau \to \ell\tau_\text{h} + \nu'\text{s}$
Trigger	Single- and double-lepton triggers	
Lepton p_T	$p_\text{T} > 25$ / 15 GeV	$p_\text{T} > 25$ / 15 (e) or 10 GeV (μ)
Lepton η	$\lvert\eta\rvert < 2.5$ (e) or 2.4 (μ)	
τ_h p_T	—	$p_\text{T} > 20$ GeV
τ_h η	—	$\lvert\eta\rvert < 2.3$
Charge requirements	2 same-sign leptons and charge quality requirements	2 same-sign leptons and charge quality requirements $\sum_{\ell,\tau_\text{h}} q = \pm 1$
Jet multiplicity	$\geq$4 jets	$\geq$3 jets
b tagging requirements	$\geq$1 tight b-tagged jet or $\geq$2 loose b-tagged jets	
Missing transverse momentum	$L_\text{D} > 30$ GeV	$L_\text{D} > 30$ GeV,*
Dilepton mass	$m_{\ell\ell} > 12$ GeV and $\lvert m_\text{ee} - m_\text{Z}\rvert > 10$ GeV,*	

Selection	3ℓ	$3\ell + 1\tau_\text{h}$
Targeted $\text{t}\bar{\text{t}}\text{H}$ decays	$\text{t} \to \text{b}\ell\nu$, $\text{t} \to \text{b}\ell\nu$, $\text{H} \to \text{WW} \to \ell\nu\text{qq}$	$\text{t} \to \text{b}\ell\nu$, $\text{t} \to \text{b}\ell\nu$, $\text{H} \to \tau\tau \to \ell\tau_\text{h} + \nu'\text{s}$
	$\text{t} \to \text{b}\ell\nu$, $\text{t} \to \text{bqq}$, $\text{H} \to \text{WW} \to \ell\nu\ell\nu$	
	$\text{t} \to \text{b}\ell\nu$, $\text{t} \to \text{bqq}$, $\text{H} \to \text{ZZ} \to \ell\ell\text{qq}$ or $\ell\ell\nu\nu$	
Trigger	Single-, double- and triple-lepton triggers	
Lepton p_T	$p_\text{T} > 25$ / 15 / 15 GeV	$p_\text{T} > 20$ / 10 / 10 GeV
Lepton η	$\lvert\eta\rvert < 2.5$ (e) or 2.4 (μ)	
τ_h p_T	—	$p_\text{T} > 20$ GeV
τ_h η	—	$\lvert\eta\rvert < 2.3$
Charge requirements	$\sum_\ell q = \pm 1$	$\sum_{\ell,\tau_\text{h}} q = 0$
Jet multiplicity	$\geq$2 jets	
b tagging requirements	$\geq$1 tight b-tagged jet or $\geq$2 loose b-tagged jets	
Missing transverse momentum	No requirement if $N_\text{j} \geq 4$ $L_\text{D} > 45$ GeV,† $L_\text{D} > 30$ GeV otherwise	
Dilepton mass	$m_{\ell\ell} > 12$ GeV and $\lvert m_{\ell\ell} - m_\text{Z}\rvert > 10$ GeV,‡	
Four-lepton mass	$m_{4\ell} > 140$ GeV,§	—

*Applied only if both leptons are electrons.
†If the event contains a SFOS lepton pair and $N_\text{j} \leq 3$.
‡Applied to all SFOS lepton pairs.
§Applied only if the event contains 2 SFOS lepton pairs.

Table 1. Event selections applied in the 2ℓss, $2\ell\text{ss} + 1\tau_\text{h}$, 3ℓ, and $3\ell + 1\tau_\text{h}$ categories.

JHEP08(2018)066

Selection	$1\ell + 2\tau_h$	4ℓ
Targeted $t\bar{t}H$ decays	$t \to b\ell\nu$, $t \to bqq$, $H \to \tau\tau \to \tau_h\tau_h + \nu$'s	$t \to b\ell\nu$, $t \to b\ell\nu$, $H \to WW \to \ell\nu\ell\nu$
		$t \to b\ell\nu$, $t \to b\ell\nu$, $H \to ZZ \to \ell\ell qq$ or $\ell\ell\nu\nu$
Trigger	Single=lepton and lepton+τ_h triggers	Single-, double- and triple-lepton triggers
Lepton p_T	$p_T > 25$ (e) or 20 GeV (μ)	$p_T > 25$ / 15 / 15 / 10 GeV
Lepton η	$\lvert\eta\rvert < 2.1$	$\lvert\eta\rvert < 2.5$ (e) or 2.4 (μ)
τ_h p_T	$p_T > 30$ / 20 GeV	—
τ_h η	$\lvert\eta\rvert < 2.3$	—
Charge requirements	$\sum_{\tau_h} q = 0$ and $\sum_{\ell,\tau_h} q = \pm 1$	—
Jet multiplicity	≥3 jets	≥2 jets
b tagging requirements	≥1 tight b-tagged jet or ≥2 loose b-tagged jets	
Dilepton mass	$m_{\ell\ell} > 12$ GeV	$m_{\ell\ell} > 12$ GeV and $\lvert m_{\ell\ell} - m_Z\rvert > 10$ GeV,[‡]
Four-lepton mass	—	$m_{4\ell} > 140$ GeV,[§]

[‡]Applied to all SFOS lepton pairs.
[§]Applied only if the event contains 2 SFOS lepton pairs.

Table 2. Event selections applied in the $1\ell + 2\tau_h$ and 4ℓ categories. If the event contains a SFOS lepton pair and $N_j \leq 3$.

is restricted to be within $|\eta| < 2.1$ to match the trigger requirements. In the $2\ell ss + 1\tau_h$ category, the leading lepton is required to satisfy $p_T > 25$ GeV, while the subleading lepton must satisfy $p_T > 15(10)$ GeV if it is an electron (or muon). In the $3\ell + 1\tau_h$ category, the leading (subleading and third) lepton is required to have $p_T > 20(10)$ GeV.

Hadronically decaying τ lepton candidates selected in the signal region of the $2\ell ss + 1\tau_h$ and $3\ell + 1\tau_h$ categories are required to pass the medium WP and must have a reconstructed $p_T > 20$ GeV. In the $1\ell + 2\tau_h$ category, the tight WP is used instead to further reduce the dominant $t\bar{t}$+jets background. The leading (subleading) τ_h candidate in this category is required to pass a threshold of $p_T > 30(20)$ GeV.

In signal events selected in the $1\ell + 2\tau_h$ category, the lepton predominantly originates from the leptonic decay of one of the top quarks, while the Higgs boson decays to a pair of τ leptons, which both decay hadronically. Consequently, we require the two τ_h to be of opposite sign, the combination of signs expected for a τ_h pair produced in a Higgs boson decay. In the $2\ell ss + 1\tau_h$ category, the sign of the reconstructed τ_h is required to be opposite to that of the leptons, while in the $3\ell + 1\tau_h$ category the sum of lepton and τ_h charges is required to be zero. Finally, the modulus of the sum of lepton charges is required to be equal to one for events selected in the 3ℓ, matching the sum of charges expected in signal events.

JHEP08(2018)066

Events selected in any category are required to contain at least one jet passing tight b tagging criteria or at least two jets passing loose b tagging criteria. Additional criteria on the multiplicity of jets are applied. In the $1\ell + 2\tau_{\mathrm{h}}$ and $2\ell\mathrm{ss} + 1\tau_{\mathrm{h}}$ categories, the presence of at least three jets, including the jets that pass the b tagging criteria, is required. The requirement on the number of jets is tightened to at least four in the 2ℓss category, consistent with the higher jet multiplicity expected in this category targeting events where the H decays into WW $\to \ell\nu\mathrm{qq}$. For events selected in the 3ℓ, $3\ell + 1\tau_{\mathrm{h}}$, and 4ℓ categories, only the presence of at least two jets is required, as those categories target events with dileptonic decay of the $\mathrm{t\bar{t}}$ pair.

In the 2ℓss and $2\ell\mathrm{ss} + 1\tau_{\mathrm{h}}$ categories, the $\mathrm{t\bar{t}}$+jets background is reduced significantly by requiring the two leptons to have the same sign. Background contributions arising from events containing two leptons of opposite sign, in which the sign of one lepton is mismeasured, are reduced by applying additional quality criteria on the charge measurement. For electrons, the consistency of the charge measurements based on different tracking algorithms and on hits reconstructed in either the silicon pixel detector or the combination of silicon pixel and strip detectors, is required. For muons, the curvature of the track reconstructed based on the combination of hits in the silicon detectors and in the muon system is required to be measured with a relative uncertainty of less than 20%.

The probability to mismeasure the charge is significantly higher for electrons than for muons. Background contributions to the 2ℓss and $2\ell\mathrm{ss} + 1\tau_{\mathrm{h}}$ categories that arise from Z+jets events in which the sign of a lepton is mismeasured are reduced by requiring events to satisfy the condition $L_{\mathrm{D}} > 30\,\mathrm{GeV}$ (applied only if both leptons are electrons in the $2\ell\mathrm{ss} + 1\tau_{\mathrm{h}}$ category) and vetoing events in which the mass of the electron pair is within 10 GeV of the Z boson mass. In the 3ℓ and $3\ell + 1\tau_{\mathrm{h}}$ categories, the background from events containing Z bosons (Z+jets, WZ, ZZ, and $\mathrm{t\bar{t}Z}$) is suppressed by requiring selected events to satisfy the condition $L_{\mathrm{D}} > 30\,\mathrm{GeV}$. The Z-veto is also extended to all events containing same-flavor opposite-sign (SFOS) lepton pairs and the requirement on L_{D} is tightened to the condition $L_{\mathrm{D}} > 45\,\mathrm{GeV}$ for those. For events with four or more jets the contamination from background processes with Z bosons is smaller and no requirement on L_{D} is applied.

In all categories, events containing lepton pairs of mass less than 12 GeV are rejected, as these events are not well modeled by the MC simulation.

In the 3ℓ and 4ℓ categories, events with two pairs of SFOS leptons passing loose identification criteria and with a 4-lepton invariant mass lower than 140 GeV are rejected, to avoid overlap with the dedicated $\mathrm{t\bar{t}H}$ category from [4].

The event selections applied in the different categories are summarized in tables 1 and 2. Combining all the event categories and assuming the SM $\mathrm{t\bar{t}H}$ production, 91 signal events are expected, corresponding to 0.5% of all produced $\mathrm{t\bar{t}H}$ events.

6 Background estimation

Contributions of background processes to the signal region (SR) of the analysis, defined by the event selection criteria detailed in section 5, arise from a variety of sources. Backgrounds

JHEP08(2018)066

are categorized as being either "reducible" or "irreducible" and are estimated either from the data or modeled using the MC simulation.

A background is considered as reducible if at least one electron or muon is due to a nonprompt lepton (i.e., originating from the decay of a hadron) or to the misidentification of a hadron, or if one or more τ_h is due to the misidentification of a quark or gluon jet. In the 2ℓss category, further sources of reducible backgrounds arise from events containing lepton pairs of opposite charge in which the sign of either lepton is mismeasured and from the production of top quark pairs in association with either real or virtual conversion photons. The dominant reducible backgrounds, arising from the misidentification of leptons or τ_h (misidentified lepton background) or from the mismeasurement of the lepton charge ("sign-flip" background), are determined from data. The procedures are described in sections 6.1 and 6.2.

The background contribution arising from $t\bar{t}$ production in association with photons ("conversions") is mostly relevant for the 2ℓss and $2\ell\text{ss}+1\tau_h$ categories. It is typically due to asymmetric conversions of the type $\gamma \to e^+e^-$, in which one electron or positron carries most of the energy of the photon, while the other electron or positron is of low energy and fails to get reconstructed. Events of this type are suppressed very effectively thanks to the electron selections used. The small remaining background is modeled using the MC simulation. The validity of the simulation has been verified in control regions (CRs) in data.

Irreducible background contributions are modeled using the MC simulation. The dominant contributions are due to the production of top quark pairs in association with W or Z bosons and to the diboson production in association with jets, dominated by the WZ and ZZ backgrounds. Minor contributions arise from rare SM processes such as triboson production, single top production in association with a Z boson, the production of two same-sign W bosons, and $t\bar{t}t\bar{t}$ production. Results are presented considering the tH process as a background process normalized to the SM expectation. The SM tH rate amounts to about 5% of the $t\bar{t}H$ one in the signal regions of this analysis. The modeling of the data by the simulation is validated in specific CRs, each enriched in the contribution of one of the dominant irreducible background processes: $t\bar{t}Z$, $t\bar{t}W$, and WZ+jets.

6.1 Background from misidentified leptons and τ_h

The background from misidentified leptons and τ_h is estimated from data by means of the fake factor (FF) method. The method is applied to each event category separately. It is based on selecting a sample of events passing all selection criteria for the respective category, detailed in section 5, except that electrons, muons, and τ_h are required to pass the relaxed, instead of nominal, selection criteria. We refer to these event samples as the "application region" (AR) of the FF method. Events in which all leptons and τ_h pass the tight selection criteria are vetoed in order to avoid overlap with the SR. An estimate for the contribution of the misidentified lepton background to the SR is obtained by applying appropriately chosen weights to the events selected in the AR.

The weights depend on the probability f_i for a misidentified electron, muon, or τ_h that passes the relaxed selection criteria to pass the nominal selection criteria. For the

JHEP08(2018)066

computation of the weights, the index i extends over all leptons and τ_{h} that pass the relaxed, but fail the nominal selection criteria. The weights differ depending on the multiplicity of leptons and τ_{h} passing the relaxed selection criteria as well as on the number of those passing the nominal selection criteria, the latter being denoted by N_{p}. For events containing a total of 2 or 3 objects, the weights are given by:

$$w_2 = \begin{cases} \frac{f_1}{1-f_1} & \text{if} \quad N_{\mathrm{p}} = 1 \\ -\frac{f_1 f_2}{(1-f_1)(1-f_2)} & \text{if} \quad N_{\mathrm{p}} = 0 \end{cases}$$

$$w_3 = \begin{cases} \frac{f_1}{1-f_1} & \text{if} \quad N_{\mathrm{p}} = 2 \\ -\frac{f_1 f_2}{(1-f_1)(1-f_2)} & \text{if} \quad N_{\mathrm{p}} = 1 \\ \frac{f_1 f_2 f_3}{(1-f_1)(1-f_2)(1-f_3)} & \text{if} \quad N_{\mathrm{p}} = 0. \end{cases} \tag{6.1}$$

The sign of the weights alternates for events with different numbers of leptons and τ_{h} candidates passing the nominal selection criteria. The alternating sign is necessary to correctly account for the contributions of events with different numbers of prompt leptons, nonprompt leptons, genuine τ_{h}, and hadrons to an event sample with a given total number of reconstructed leptons and τ_{h}. For example, in the case of events with two leptons in the 2ℓss category, the negative sign in the expression $-f_1 f_2/[(1-f_1)(1-f_2)]$ for the weight w_2 corrects for the contribution of events with two nonprompt leptons or misidentified hadrons to the sample of events in which one lepton passes and the other one fails the nominal lepton selection criteria. Application of the weights given by eq. (6.1) to events in the AR provides an unbiased estimate of the background contribution in the SR arising from events with at least one nonprompt lepton or hadron misidentified as prompt lepton or τ_{h}. A correction obtained from the MC simulation is subtracted from this estimate to account for the contamination of the AR with irreducible backgrounds, i.e., by events in which all leptons are prompt leptons and all τ_{h} are genuine, and in which a prompt lepton fails the nominal lepton selection criteria or a genuine τ_{h} fails the nominal τ_{h} selection criteria. The correction does not exceed 10% of the yield in the AR in any category.

The factors f_i are measured separately for electrons, muons, and τ_{h} and are parametrized as functions of p_{T} and η. The CR in which the f_i are measured is referred to as "determination region" (DR) of the FF method. The f_i for electrons and muons are measured in multijet events. Selected events are required to contain one electron or muon passing the relaxed lepton selection criteria and at least one jet. The data in this DR are collected with single lepton triggers, except at low muon p_{T}, where the presence of an additional jet with $p_{\mathrm{T}} > 40\,\mathrm{GeV}$ is required in the trigger. Contamination from prompt leptons, primarily arising from the production of single W and Z bosons in association with jets, with a small contribution from diboson production, is reduced by vetoing events with multiple leptons. The residual contamination is subtracted based on a likelihood fit, similar to the one used for measuring the $\mathrm{t\bar{t}H}$ production rate in the SR described in section 7, that determines the relative contributions of different background processes with prompt leptons to the DR. A variable closely related to the transverse mass of the electron or muon

JHEP08(2018)066

and $\vec{p}_{\mathrm{T}}^{\,\mathrm{miss}}$,

$$m_{\mathrm{T}}^{'} = \sqrt{2 p_{\mathrm{T}\ell}^{\mathrm{fix}}\, p_{\mathrm{T}}^{\mathrm{miss}}\ (1 - \cos\Delta\phi)}, \tag{6.2}$$

is used as the discriminating observable in the fit. Here, $p_{\mathrm{T}\ell}^{\mathrm{fix}} = 35\,\mathrm{GeV}$ is used to reduce the correlation between $m_{\mathrm{T}}^{'}$ and the p_{T} of the lepton and $\Delta\phi$ denotes the angle in the transverse plane between the lepton momentum and the $\vec{p}_{\mathrm{T}}^{\,\mathrm{miss}}$ vector. A complication arises from the fact that the factors f_i are measured in multijet events, while the dominant misidentified lepton background in the AR is due to $\mathrm{t\bar{t}}$+jets production. The relaxed lepton selection criteria are chosen such that the f_i are similar for nonprompt leptons and for hadrons that are misidentified as prompt leptons and do not differ between multijet and $\mathrm{t\bar{t}}$+jets events. The f_i for τ_{h} are measured using $\mathrm{t\bar{t}}$+jets events in which the two W bosons produced in the decay of the top quark pair decay to an electron-muon pair. The events are required to contain one electron, one muon, at least one τ_{h} candidate passing the relaxed τ_{h} selection, and two or more jets, of which at least one passes the tight or at least two pass the loose b tagging criteria, and are recorded by a combination of single-lepton triggers and triggers based on the presence of an electron-muon pair. Contributions from other background processes are reduced by requiring the observable L_{D}, defined by eq. (4.4), to satisfy the condition $L_{\mathrm{D}} > 30\,\mathrm{GeV}$. The contamination from background processes with genuine τ_{h} is subtracted using the MC simulation. Separate sets of f_i are measured for the τ_{h} selection criteria applied in the $2\ell\mathrm{ss}{+}1\tau_{\mathrm{h}}$ and $3\ell{+}1\tau_{\mathrm{h}}$ categories and for those applied in the $1\ell{+}2\tau_{\mathrm{h}}$ category.

For the $1\ell{+}2\tau_{\mathrm{h}}$, $2\ell\mathrm{ss}$ and 3ℓ categories, the FF method is applied as described, whereas a modified version of the FF method is utilized in the $2\ell\mathrm{ss} + 1\tau_{\mathrm{h}}$ and $3\ell + 1\tau_{\mathrm{h}}$ categories. In the modified version, only the part of the misidentified lepton background in which at least one of the reconstructed electrons or muons is misidentified is obtained from data, relaxing only the selection criteria for electrons and muons when defining the AR. On the other hand, the contribution of background events that contain genuine prompt light leptons and in which the reconstructed τ_{h} is due to the misidentification of a quark or gluon jet is obtained from the MC simulation, corrected to account for the difference in the τ_{h} misidentification probability in data and simulation. In this way, $\mathrm{t\bar{t}H}$ events where the reconstructed τ_{h} is not due to a genuine τ_{h} can be retained as signal, instead of being included in the misidentified lepton background estimate. These events amount to $\approx 30\%$ of the total signal in the $2\ell\mathrm{ss} + 1\tau_{\mathrm{h}}$ and $3\ell + 1\tau_{\mathrm{h}}$ categories.

We have checked that the background due to nonprompt leptons was negligible in the 4ℓ category and the FF method is therefore not used in this category.

6.2 Sign-flip background

The sign-flip background in the $2\ell\mathrm{ss}$ and $2\ell\mathrm{ss} + 1\tau_{\mathrm{h}}$ categories is dominated by $\mathrm{t\bar{t}}$+jets events with two prompt leptons in which the sign of either prompt lepton is mismeasured. The background is estimated from data, following a strategy similar to the one used for the estimation of the misidentified lepton background. The AR used to estimate the contribution of the sign-flip background to the SR contains events passing all selection criteria of the SR, described in section 5, of the respective category, except that the two

JHEP08(2018)066

leptons are required to be of opposite sign. In the 2ℓss category, the sum of the probabilities to mismeasure the charge of either one of the two leptons is then applied as an event weight. In the $2\ell\text{ss} + 1\tau_\text{h}$ category, only the probability to mismeasure the sign of the lepton with the same sign as the τ_h is used, due to the charge requirements used for the event selection in this category. The sign misidentification rates for electrons and muons are measured by comparing the rates of $\text{Z}/\gamma^* \to \text{ee}$ and $\text{Z}/\gamma^* \to \mu\mu$ events with leptons of the same and of opposite sign and are parametrized as functions of lepton p_T and η. The probability for mismeasuring the sign of electrons ranges from 0.02% for electrons in the barrel to 0.4% for electrons in the endcaps, after all the object selection criteria. The probability for mismeasuring the sign of muons is negligible in this analysis.

7 Signal extraction

The event samples selected in the SR are still dominated by backgrounds in all event categories. The sensitivity of the statistical analysis is enhanced by extracting the signal rate by means of a maximum likelihood (ML) fit to the distribution in a discriminating observable, except in the 4ℓ category, where we resort to event counting because of the small number of events expected in this category. In each event category, a different discriminating observable is chosen, in order to achieve the maximal separation in shape between the $\text{t}\bar{\text{t}}\text{H}$ signal and backgrounds. The observables used for the ML fit are described in section 7.1, and the statistical analysis is detailed in section 7.2.

7.1 Discriminating observables

Discriminants based on the MEM approach have been developed for the $2\ell\text{ss} + 1\tau_\text{h}$ and 3ℓ categories to improve the separation of the $\text{t}\bar{\text{t}}\text{H}$ signal with respect to the main backgrounds. The computation of the discriminant is based on combining the knowledge of differential theoretical cross sections for the $\text{t}\bar{\text{t}}\text{H}$ signal and for background processes with the knowledge of the experimental resolution of the detector. More details about their computations are provided in appendix A.

In the $2\ell\text{ss} + 1\tau_\text{h}$ category, a MEM discriminant $\text{LR}(2\ell\text{ss} + 1\tau_\text{h})$ is directly used for the signal extraction, optimized to discriminate the $\text{t}\bar{\text{t}}\text{H}$ signal from three types of background: $\text{t}\bar{\text{t}}\text{Z}$ events in which the Z boson decays into a pair of τ leptons, $\text{t}\bar{\text{t}}\text{Z}$ events in which the Z boson decays into a pair of electrons or muons and one lepton is misidentified as τ_h, and $\text{t}\bar{\text{t}} \to \text{b}\ell\nu\,\bar{\text{b}}\tau\nu$ events with one additional nonprompt lepton produced in either a b or a $\bar{\text{b}}$ quark decay.

The discriminating observable used for the signal extraction in each of the categories 2ℓss, 3ℓ, and $3\ell + 1\tau_\text{h}$ is based on the output of two BDTs. The first BDT is trained to separate the $\text{t}\bar{\text{t}}\text{H}$ signal from the $\text{t}\bar{\text{t}}\text{V}$ background and the second to separate the signal from the $\text{t}\bar{\text{t}}$+jets background. In the $1\ell + 2\tau_\text{h}$ category, the background is largely dominated by $\text{t}\bar{\text{t}}$+jets production and a single BDT is trained to separate the signal from this background.

The training of the BDTs is performed on simulated events. The events used for the training are not used elsewhere in the analysis. The observables used as input to the BDTs are summarized in table 3. The choice of input variables is optimized for each category

JHEP08(2018)066

Observable	$1\ell + 2\tau_{\mathrm{h}}$	$2\ell\mathrm{ss}$	3ℓ	$3\ell + 1\tau_{\mathrm{h}}$
$\Delta R(\ell_1, \mathrm{j})$	—	√	√	√
$\Delta R(\ell_2, \mathrm{j})$	—	√	√	√
$\langle \Delta R_{\mathrm{jj}} \rangle$	√	—	—	√,[2]
$\Delta R_{\tau\tau}$	√	—	—	—
$\max\left(\lvert\eta^{\ell 1}\rvert, \lvert\eta^{\ell 2}\rvert\right)$	—	√	√	√
$H_{\mathrm{T}}^{\mathrm{miss}}$	√	—	—	√,[2]
N_{j}	√	√	√	√
N_{b}	√	—	—	—
$m_{\tau\tau}^{\mathrm{vis}}$	√	—	—	—
$m_{\mathrm{T}}^{\ell 1}$	—	√	√	√
$p_{\mathrm{T}}^{\ell 1}$	—	√,[1]	√,[1]	√,[1]
$p_{\mathrm{T}}^{\ell 2}$	—	√,[1]	-	-
$p_{\mathrm{T}}^{\ell 3}$	—	—	√,[1]	√,[1]
$p_{\mathrm{T}}^{\tau 1}$	√	—	—	—
$p_{\mathrm{T}}^{\tau 2}$	√	—	—	—
$\mathrm{LR}(3\ell)$	—	—	√,[1]	—
$\mathrm{MVA}_{\mathrm{thad}}^{\mathrm{max}}$	—	√,[2]	—	—
$\mathrm{MVA}_{\mathrm{Hj}}^{\mathrm{max}}$	—	√,[1]	—	—

[1]Used only in BDT that separates $\mathrm{t\bar{t}H}$ signal from $\mathrm{t\bar{t}V}$ background.
[2]Used only in BDT that separates $\mathrm{t\bar{t}H}$ signal from $\mathrm{t\bar{t}}$+jets background.

Table 3. Observables used as input to the BDTs that separate the $\mathrm{t\bar{t}H}$ signal from the $\mathrm{t\bar{t}V}$ and $\mathrm{t\bar{t}}$+jets backgrounds in the $1\ell + 2\tau_{\mathrm{h}}$, $2\ell\mathrm{ss}$, 3ℓ, and $3\ell + 1\tau_{\mathrm{h}}$ categories.

individually, and separate optimizations are performed for the BDT that separates the signal from the $\mathrm{t\bar{t}V}$ background and the one that separates the signal from the $\mathrm{t\bar{t}}$+jets background.

The input variables given in the table are defined as follows:

- $\Delta R(\ell_1, \mathrm{j})$ ($\Delta R(\ell_2, \mathrm{j})$) refers to the separation between the leading (subleading) lepton and the nearest jet;
- $\langle \Delta R_{\mathrm{jj}} \rangle$ refers to the average distance between jets;
- $\Delta R_{\tau\tau}$ refers to the distance between the leading and subleading τ_{h};
- N_{j} and N_{b} refer to the number of jets and b-tagged jets of 25 GeV and $|\eta| < 2.4$ that do not overlap, within $R < 0.4$, with any electron, muon, or τ_{h} passing the relaxed selection criteria;
- $m_{\tau\tau}^{\mathrm{vis}}$ refers to the visible mass of the leading and subleading τ_{h};

JHEP08(2018)066

- $m_{\mathrm{T}}^{\ell 1}$ refers to the transverse mass of the leading lepton and the $\vec{p}_{\mathrm{T}}^{\,\mathrm{miss}}$ vector, computed according to eq. (6.2);

- $p_{\mathrm{T}}^{\ell 1}$ ($p_{\mathrm{T}}^{\ell 2}$, $p_{\mathrm{T}}^{\ell 3}$) refers to the p_{T} of the leading (subleading, third) lepton;

- $p_{\mathrm{T}}^{\tau 1}$ ($p_{\mathrm{T}}^{\tau 2}$) refers to the p_{T} of the leading (subleading) τ_{h};

- LR(3ℓ) refers to a MEM discriminant for the 3ℓ category, optimized to discriminate the $\mathrm{t\bar{t}H}$ signal from the two dominant irreducible background processes $\mathrm{t\bar{t}Z}$ and $\mathrm{t\bar{t}W}$;

- The observable $\mathrm{MVA}_{\mathrm{thad}}^{\mathrm{max}}$ quantifies the compatibility of jets with a hadronic decay of a top quark. The compatibility is computed as the response of a BDT classifier and evaluated for each possible jet and lepton permutation, using several kinematic quantities and b tagging information as inputs. The maximum over all those permutations is used as input to the BDT that separates the $\mathrm{t\bar{t}H}$ signal from the $\mathrm{t\bar{t}}$+jets background in the 2ℓss category;

- The observable $\mathrm{MVA}_{\mathrm{Hj}}^{\mathrm{max}}$ quantifies the compatibility of jets to originate from $\mathrm{H} \to \mathrm{WW}^*$ decays in which one W boson decays leptonically and the other to a pair of quarks. The compatibility is computed as the response of a BDT classifier and evaluated per jet, using angular variables and jet identification variables (b tagging and quark-gluon discriminants). The maximum over all jets is used as input to the BDT that separates the $\mathrm{t\bar{t}H}$ signal from the $\mathrm{t\bar{t}V}$ background in the 2ℓss category. Jets that are compatible with originating from the hadronic decays of top quarks according to $\mathrm{MVA}_{\mathrm{thad}}^{\mathrm{max}}$ are excluded from the computation of $\mathrm{MVA}_{\mathrm{Hj}}^{\mathrm{max}}$.

The outputs of the two BDTs that separate the $\mathrm{t\bar{t}H}$ signal from the $\mathrm{t\bar{t}V}$ and $\mathrm{t\bar{t}}$+jets backgrounds are mapped into a single discriminant $\mathrm{D_{MVA}}$ that is used as a discriminating observable for the signal extraction in the 2ℓss, 3ℓ, and $3\ell + 1\tau_{\mathrm{h}}$ categories. The mapping is determined as follows. The algorithm starts by filling two-dimensional histograms of the output of the first versus the second BDT for signal and background events. The histograms use a fine binning. The distributions for signal and for background are smoothed using Gaussian kernels to reduce statistical fluctuations. The ratio of signal to background event yields is computed in each bin and assigned to background events depending on the bins they fall in. The cumulative distribution of this ratio is produced for background events and partitioned, based on its quantiles, into N regions of equal background content. The number of regions is chosen using a recursive application of the k-means clustering algorithm with $k = 2$ [58] on the two-dimensional distribution of the BDTs, including stopping conditions limiting the statistical uncertainty in the signal and background templates. The output of the algorithm that determines the mapping is a partitioning of the two-dimensional plane spanned by the output of the two BDTs into N regions and an enumeration, used as a discriminant, of these regions by increasing signal-to-background ratio. By construction, the distribution of the background is approximately flat in this discriminant, while the distribution of the signal increases from low to high values of the discriminant. In the 2ℓss and 3ℓ categories, the signal extraction is performed using this

JHEP08(2018)066

discriminant in subcategories based on lepton flavor, lepton charges and b-tagging requirements. In the $3\ell + 1\tau_{\mathrm{h}}$ category, due to limited statistics in simulation, the training of the two BDTs and the two-dimensional mapping have been actually performed with an inclusive 3ℓ selection, resulting in a non flat background distribution.

Events selected in the $2\ell\mathrm{ss} + 1\tau_{\mathrm{h}}$ category are analyzed in two subcategories, motivated by different signal-to-background ratios and different levels of signal-to-background separation provided by the MEM discriminant $\mathrm{LR}(2\ell\mathrm{ss}+1\tau_{\mathrm{h}})$ in each of the subcategories. The "no-missing-jet" subcategory contains events in which a pair of jets compatible with originating from the hadronic decay of a W boson is reconstructed, which allows for a full reconstruction of the decay chain $\mathrm{t\bar{t}H} \to \mathrm{bW\,\bar{b}W}\,\tau\tau \to \mathrm{bjj\,\bar{b}}\ell\nu\,\ell\bar{\nu}_{\ell}\nu_{\tau}\,\tau_{\mathrm{h}}\bar{\nu}_{\tau}$ in signal events, while the "missing-jet" category contains events with no such pair of jets. The full reconstruction of the decay chain improves the separation of the $\mathrm{t\bar{t}H}$ signal from background events. Signal events can contribute to the "missing-jet" category if, for example, one of the jets produced in the W boson decay is outside of the p_{T} and η acceptance or if it overlaps with another jet.

7.2 Statistical analysis

The rate of the $\mathrm{t\bar{t}H}$ signal μ is measured through a simultaneous ML fit to the distribution in the discriminating observables or the number of events observed in the six event categories $1\ell+2\tau_{\mathrm{h}}$, $2\ell\mathrm{ss}$, $2\ell\mathrm{ss}+1\tau_{\mathrm{h}}$, 3ℓ, $3\ell+1\tau_{\mathrm{h}}$, and 4ℓ. The best-fit value of this parameter is denoted as $\hat{\mu}$. A 68% confidence interval on the parameter of interest is obtained using a maximum likelihood fit based on the profile likelihood ratio test statistic [59, 60]. A potential signal excess in data is quantified by calculating the corresponding p-value. Upper limits on the $\mathrm{t\bar{t}H}$ signal rate are set via the CL_s method [61, 62].

The nuisance parameters described in section 8 are treated via the frequentist paradigm, as described in refs. [59, 60]. Systematic uncertainties that affect only the normalization, but not the distribution in any discriminating observable, are represented by Γ-function distributions if they are statistical in origin, e.g., corresponding to the number of events observed in a control region, and by log-normal probability density functions otherwise. Systematic uncertainties that affect the distribution in the discriminating observables are incorporated into the ML fit via the technique detailed in ref. [63], and represented by Gaussian probability density functions. Nuisance parameters representing systematic uncertainties of the latter type can also affect the normalization of the $\mathrm{t\bar{t}H}$ signal or of the backgrounds.

8 Systematic uncertainties

Various imprecisely measured or simulated effects can affect the rates as well as the distributions of the observables used for the signal extraction, described in section 7. We differentiate the corresponding systematic uncertainties between experimental and theory-related sources. The contributions of background processes that are determined from data, as described in section 6, are mostly unaffected by potential inaccuracies of the MC simulation.

JHEP08(2018)066

The efficiency for events to pass the combination of triggers based on the presence of one, two, or three electrons or muons is measured in bins of lepton multiplicity with an uncertainty between 1 and 3% using a sample of events recorded by triggers based on $p_{\mathrm{T}}^{\mathrm{miss}}$. The efficiency of the trigger that selects events containing an electron or muon in combination with a τ_{h} in the $1\ell + 2\tau_{\mathrm{h}}$ category is measured with an uncertainty of 3% in $\mathrm{Z}/\gamma^* \to \tau\tau$ events.

The efficiencies to reconstruct and identify electrons and muons are measured as a function of p_{T} with uncertainties ranging from 2 to 4% using $\mathrm{Z}/\gamma^* \to \mathrm{ee}$ and $\mathrm{Z}/\gamma^* \to \mu\mu$ events via the tag-and-probe method discussed in ref. [64]. The τ_{h} reconstruction and identification efficiency and the τ_{h} energy scale are measured with uncertainties of 5 and 3%, respectively, using $\mathrm{Z}/\gamma^* \to \tau\tau$ events [41].

The energy scale of jets is measured using the p_{T} balance of jets with Z bosons and photons in $\mathrm{Z}/\gamma^* \to \mathrm{ee}$ and $\mathrm{Z}/\gamma^* \to \mu\mu$ and γ+jets events and the p_{T} balance between jets in dijet and multijet events [55]. The uncertainty in the jet energy scale is a few percent and depends on p_{T} and η. The impact of jet energy scale uncertainties on event yields and on the distributions in kinematic observables is evaluated by varying the jet energy corrections within their uncertainties and propagating the effect to the final result by recalculating all kinematic quantities, including $p_{\mathrm{T}}^{\mathrm{miss}}$, $H_{\mathrm{T}}^{\mathrm{miss}}$, and L_{D}, and reapplying all event selection criteria.

The b tagging efficiencies are measured in multijet events, enriched in the heavy-flavor content by requiring the presence of a muon, and in $\mathrm{t\bar{t}}$+jets events, with uncertainties of a few percent, depending on p_{T} and η [57]. The mistag rates for light-quark and gluon jets are measured in Z+jets events with an uncertainty of 5–10% for the loose and 20–30% for the tight b tagging criteria, again depending on p_{T} and η [57].

The uncertainty in the integrated luminosity amounts to 2.5% [65].

Uncertainties from theoretical sources are assigned to the $\mathrm{t\bar{t}V}$ backgrounds and to the signal normalization. The cross sections of the irreducible $\mathrm{t\bar{t}Z}$, $\mathrm{t\bar{t}W}$, and $\mathrm{t\bar{t}WW}$ backgrounds are known with uncertainties of $^{+9.6\%}_{-11.2\%}$, $^{+12.9\%}_{-11.5\%}$, and $^{+8.1\%}_{-10.9\%}$, respectively, from missing higher-order corrections on the perturbative expansion and of 3.4, 4 and 3%, respectively, from uncertainties in the PDFs and in the strong coupling constant α_s [66]. The theoretical uncertainties in the SM expectation for the $\mathrm{t\bar{t}H}$ signal cross section amount to $^{+5.8\%}_{-9.3\%}$ from missing higher-order corrections on the perturbative expansion and to 3.6% from uncertainties in the PDFs and in α_s [66]. The effect of missing higher orders on distributions in kinematic observables is evaluated through independent changes in the renormalization and factorization scales by factors of 2 and 1/2 relative to their nominal equal values [67–69].

The estimate for the misidentified lepton background, obtained from data as described in section 6.1, is subject to uncertainties in the factors f_i that are used to compute the event weights in eq. (6.1). The impact of these uncertainties is separated into effects on the normalization and on the shape of the distributions used for signal extraction. The effect on the normalization ranges from 10 to 40%, depending on the multiplicity of misidentified electrons, muons, and τ_{h}, and on their p_{T} and η. The uncertainties in the normalization include the effect of statistical uncertainties in the sample used to measure the f_i, of

JHEP08(2018)066

systematic uncertainties related to the subtraction of the prompt-lepton contamination in this sample, and of the non-perfect agreement in simulation between distributions for misidentified lepton background and those obtained when applying the FF method. The effect on distributions in kinematic observables is computed as follows. In case of electrons and muons, an uncertainty band for the distributions used for signal extraction is obtained by applying independent variations of the f_i in different bins of p_{T} and η. In case of τ_{h}, we fit the misidentification rates f_i measured in the barrel and endcap region of the detector as function of p_{T} and propagate the uncertainty in the slope of the fit to the final result, in a correlated way between all the categories with τ_{h} candidates, with typical values around 3%.

The uncertainty in the sign misidentification rate for electrons is propagated to the final result in a similar way. The corresponding uncertainty in the rate of the sign-flip background amounts to $\approx 30\%$.

Even though the WZ production is predicted theoretically at NLO accuracy and its inclusive cross section has been measured successfully at the LHC [70, 71], this good agreement does not translate automatically to the signal regions considered for this analysis, which require the presence of at least one b-tagged jet. A conservative 100% uncertainty is therefore assigned to the diboson background in all categories but the 3ℓ one. The uncertainty is reduced to $\approx 40\%$ for the 3ℓ categories from studies in a dedicated 3ℓ WZ CR, defined by inverting the Z veto on the dilepton mass and the b tagging requirement. The overall uncertainty assigned to the diboson prediction in that case is estimated from the statistical uncertainty due to the limited sample size in the CR (30%), the residual background in the CR (20%), the uncertainties in the b tagging rate (between 10 and 40%), and from the knowledge of PDFs and the theoretical uncertainties in the flavor composition of the jets produced in association with the electroweak bosons (up to 10%).

An uncertainty of 50% is assigned to the rate of other minor backgrounds. This conservative uncertainty accounts for the fact that the small background contributions from those processes have not yet been measured at the LHC.

Among all the sources of uncertainty listed above, the ones having the largest impact on the measured $\mathrm{t\bar{t}H}$ signal rate are related to the lepton efficiency measurement, the estimate of the misidentified lepton background and the theoretical sources affecting the normalization of the signal and irreducible backgrounds, as can be seen from table 4. The systematic uncertainties related to the lepton efficiency measurement and the estimate of the misidentified lepton background are treated as correlated between all the categories which include leptons with a given flavor. The systematic uncertainties in the normalization of the signal and irreducible backgrounds are treated as correlated between all the categories.

9 Results

The number of events observed in the different categories are compared to the SM expectations after the ML fit in table 5. The event yields resulting from the fit are consistent with those predicted by the original background and signal estimates within the uncertainties

JHEP08(2018)066

Source	Uncertainty [%]	$\Delta\mu/\mu$ [%]
e, μ selection efficiency	2–4	11
τ_h selection efficiency	5	4.5
b tagging efficiency	2–15 [57]	6
Reducible background estimate	10–40	11
Jet energy calibration	2–15 [55]	5
τ_h energy calibration	3	1
Theoretical sources	≈10	12
Integrated luminosity	2.5	5

Table 4. Summary of the main sources of systematic uncertainty and their impact on the combined measured $t\bar{t}H$ signal rate μ. $\Delta\mu/\mu$ corresponds to the relative shift in signal strength obtained from varying the systematic source within its associated uncertainty.

described in section 8. Most of those uncertainties are not very constrained by the ML fit, except for the uncertainty related to the background due to jets misidentified as τ_h candidates. This originates from the $1\ell + 2\tau_h$ category which is dominated by this background. Distributions in the discriminating observables used for the signal extraction in the different categories after the final fit are shown in figures 2–4. In figure 5, the different bins of the distributions are classified according to their expected ratio of signal (S) to background (B) events. An excess of observed events with respect to the SM backgrounds is visible in the most sensitive bins.

Upper limits on the signal rate, computed at 95% confidence level (CL), are given in table 6. The limits are computed for separate fits of each category, and for their combination. The observed limit computed from the combination of all categories amounts to 2.1 times the SM $t\bar{t}H$ production rate. The observed limit is compatible with the one expected if a SM $t\bar{t}H$ signal is present at the SM predicted rate, amounting to 1.7 times the SM $t\bar{t}H$ production rate in the presence of a $t\bar{t}H$ signal. In the absence of signal, an upper limit on the signal rate of 0.8 times the SM $t\bar{t}H$ production rate is expected.

Signal yields are extracted from a fit with μ allowed to assume different values in each category, or constrained to assume the same value in all the categories for the combined result. The results are shown in figure 6. For the combined fit, the observed (expected) signal rate is $\mu = 1.23^{+0.45}_{-0.43}$ $(1.00^{+0.42}_{-0.38})$ times the SM $t\bar{t}H$ production rate, with an observed (expected) significance of 3.2σ (2.8σ), which represents evidence for $t\bar{t}H$ production in those final states. While the categories 2ℓss, 3ℓ and 4ℓ are mostly sensitive to the $t\bar{t}H$ signal in the $H \to WW$ and $H \to ZZ$ decay modes, the $1\ell + 2\tau_h$, $2\ell\text{ss} + 1\tau_h$ and $3\ell + 1\tau_h$ categories enhance the sensitivity to the $H \to \tau\tau$ decay mode. The distributions in the discriminating observables are very similar for $t\bar{t}H$ signal events with a H boson decaying into W bosons, Z bosons, and τ leptons, however, causing a large anti-correlation between the corresponding signal rates. Denoting the sum of $H \to WW$ and $H \to ZZ$ decay

JHEP08(2018)066

Process	$1\ell + 2\tau_h$	2ℓss	2ℓss $+ 1\tau_h$
$t\bar{t}H$	7.1 ± 2.4	66.3 ± 21.0	11.6 ± 3.5
$t\bar{t}Z/\gamma^*$	6.3 ± 1.1	80.9 ± 10.4	9.2 ± 1.2
$t\bar{t}W + t\bar{t}WW$	0.5 ± 0.1	150.0 ± 16.9	9.1 ± 1.0
WZ + ZZ	2.1 ± 1.6	16.5 ± 13.1	3.9 ± 3.0
tH	0.4 ± 0.1	2.7 ± 0.2	0.5 ± 0.04
Conversions	< 0.02	12.1 ± 5.8	1.4 ± 0.5
Sign flip	—	27.5 ± 8.0	0.5 ± 0.1
Misidentified leptons	195.7 ± 13.6	94.2 ± 21.2	8.6 ± 2.1
Rare backgrounds	1.4 ± 0.7	39.0 ± 21.2	3.1 ± 1.5
Total expected background	206.3 ± 14.0	423.0 ± 38.0	36.1 ± 4.2
Observed	212	507	49

Process	3ℓ	$3\ell + 1\tau_h$	4ℓ
$t\bar{t}H$	22.8 ± 7.4	2.6 ± 0.9	1.1 ± 0.4
$t\bar{t}Z/\gamma^*$	49.0 ± 6.9	3.4 ± 0.5	2.1 ± 0.4
$t\bar{t}W + t\bar{t}WW$	35.2 ± 4.2	0.4 ± 0.04	$< 2 \times 10^{-3}$
WZ + ZZ	9.9 ± 2.4	0.3 ± 0.05	0.1 ± 0.1
tH	1.2 ± 0.2	0.1 ± 0.01	$< 4 \times 10^{-4}$
Conversions	5.3 ± 2.9	< 0.02	< 0.02
Misidentified leptons	22.7 ± 6.7	0.9 ± 0.2	< 0.04
Rare backgrounds	8.2 ± 13.8	0.2 ± 0.1	0.1 ± 0.2
Total expected background	131.4 ± 18.2	5.3 ± 0.5	2.4 ± 0.4
Observed	148	7	3

Table 5. Numbers of events selected in the different categories compared to the SM expectations for the $t\bar{t}H$ signal and background processes. The event yields expected for the $t\bar{t}H$ signal and for the backgrounds are shown for the values of nuisance parameters obtained from the combined ML fit and $\mu = \hat{\mu} = 1.23$. Quoted uncertainties represent the combination of statistical and systematic components.

JHEP08(2018)066

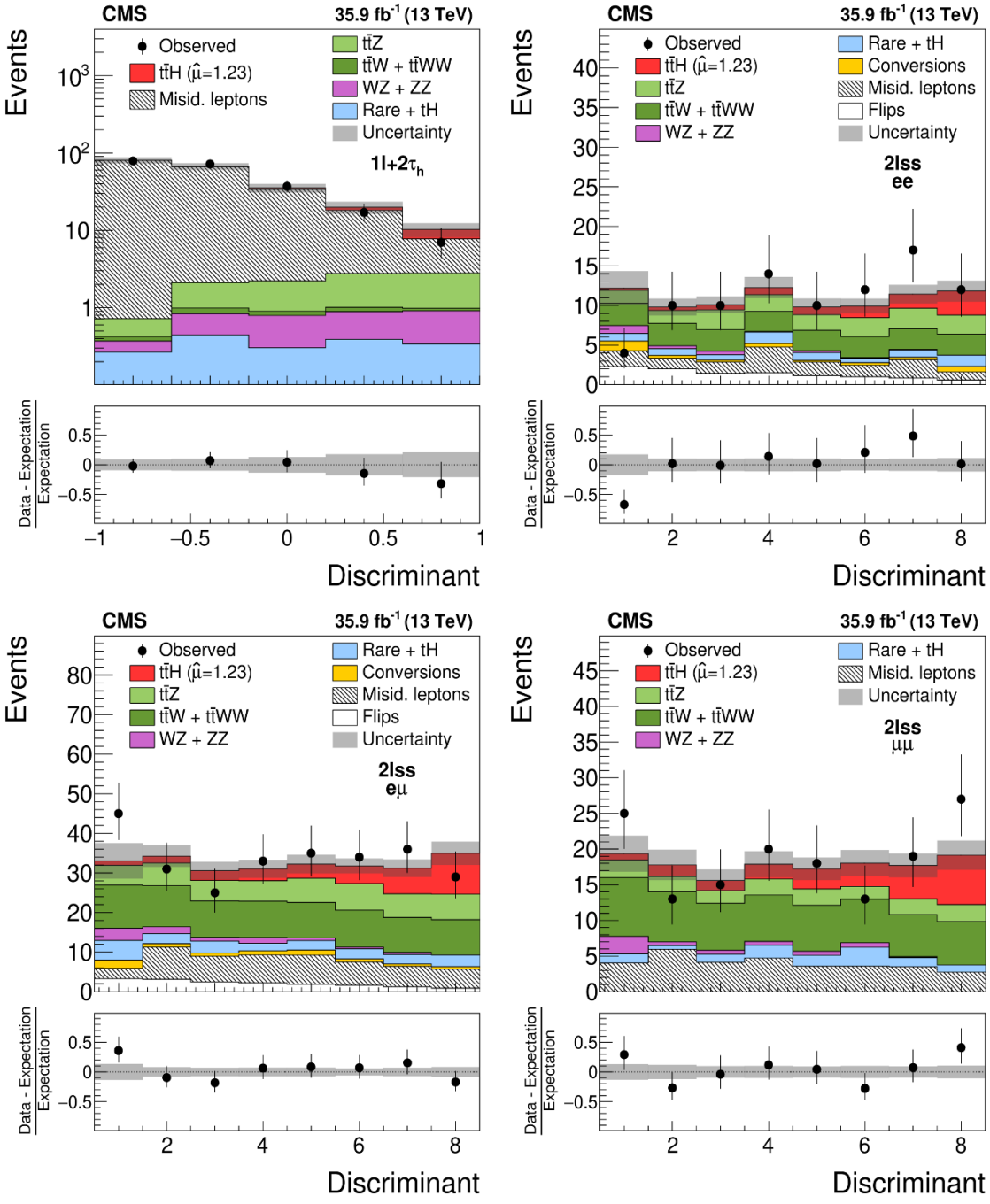

Figure 2. Distributions in the discriminating observables used for the signal extraction in the $1\ell+2\tau_h$ category (top left) and in different subcategories of the 2ℓss category (top right and bottom row), compared to the SM expectation for the $t\bar{t}H$ signal and for background processes. A BDT trained to separate the $t\bar{t}H$ signal from the $t\bar{t}$+jets background is used in the $1\ell+2\tau_h$ category, while a D_{MVA} variable, combining the outputs of two BDTs trained to discriminate the $t\bar{t}H$ signal from the $t\bar{t}V$ and $t\bar{t}$+jets backgrounds respectively, is used in the 2ℓss subcategories. The distributions expected for signal and background processes are shown for the values of nuisance parameters obtained from the combined ML fit and $\mu = \hat{\mu} = 1.23$, corresponding to the best-fit value from the ML fit.

JHEP08(2018)066

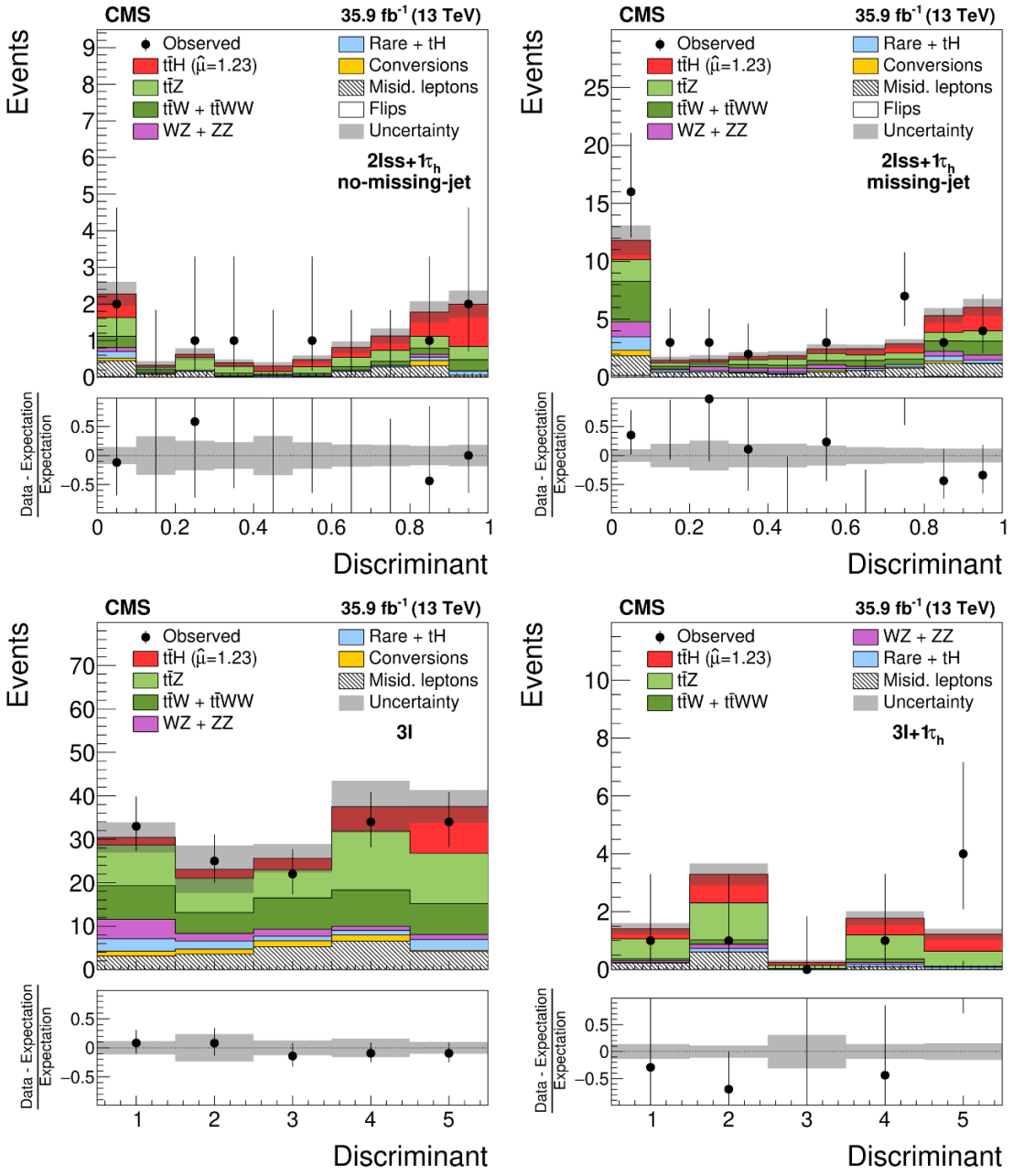

Figure 3. Distributions in the discriminating observables used for the signal extraction in the "no-missing-jet" (top left) and "missing-jet" (top right) subcategories of the $2\ell\mathrm{ss}+1\tau_\mathrm{h}$ category, the 3ℓ category (bottom left), and the $3\ell+1\tau_\mathrm{h}$ category (bottom right), compared to the SM expectation for the $\mathrm{t\bar{t}H}$ signal and for background processes. The MEM discriminant $\mathrm{LR}(2\ell\mathrm{ss}+1\tau_\mathrm{h})$ is used in the $2\ell\mathrm{ss}+1\tau_\mathrm{h}$ subcategories, while a $\mathrm{D_{MVA}}$ variable, combining the outputs of two BDTs trained to discriminate the $\mathrm{t\bar{t}H}$ signal from the $\mathrm{t\bar{t}V}$ and $\mathrm{t\bar{t}}$+jets backgrounds respectively, is used in the 3ℓ and $3\ell+1\tau_\mathrm{h}$ categories. The distributions expected for signal and background processes are shown for the values of nuisance parameters obtained from the combined ML fit and $\mu=\hat{\mu}=1.23$, corresponding to the best-fit value from the ML fit. The lowest bin of the MEM discriminant in the "missing-jet" subcategory of the $2\ell\mathrm{ss}+1\tau_\mathrm{h}$ category collects events for which the kinematics of the reconstructed objects is not compatible with the $\mathrm{t\bar{t}H}$, $\mathrm{H}\to\tau\tau$ signal hypothesis.

JHEP08(2018)066

Category	Observed limit on μ	Expected limit	
		$(\mu = 0)$	$(\mu = 1)$
$1\ell + 2\tau_h$	2.7	$4.1^{+1.7}_{-1.4}$	$4.8^{+2.0}_{-1.9}$
2ℓss	2.8	$1.0^{+0.4}_{-0.2}$	$2.0^{+0.7}_{-0.3}$
2ℓss $+ 1\tau_h$	2.5	$1.4^{+0.7}_{-0.3}$	$2.5^{+0.9}_{-0.5}$
3ℓ	2.7	$1.6^{+0.8}_{-0.4}$	$2.9^{+1.1}_{-0.4}$
$3\ell + 1\tau_h$	4.4	$2.8^{+1.3}_{-0.6}$	$4.1^{+1.5}_{-0.7}$
4ℓ	6.5	$4.9^{+2.8}_{-1.1}$	$6.7^{+2.5}_{-0.8}$
Combined	2.1	$0.8^{+0.3}_{-0.2}$	$1.7^{+0.5}_{-0.5}$

Table 6. The 95% CL upper limits on the $t\bar{t}H$ signal rate, in units of the SM $t\bar{t}H$ production rate, obtained in each of the categories individually and for the combination of all six event categories. The observed limit is compared to the limits expected for the background-only hypothesis ($\mu = 0$) and for the case that a $t\bar{t}H$ signal of SM production rate is present in the data ($\mu = 1$). The ± 1 standard deviation uncertainty intervals on the expected limits are also given in the table.

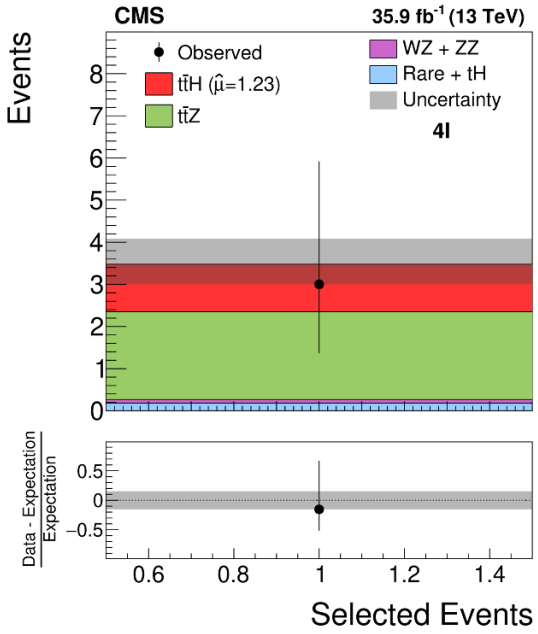

Figure 4. Number of events observed and expected in the 4ℓ category. The distributions expected for signal and background processes are shown for the values of nuisance parameters obtained from the combined ML fit and $\mu = \hat{\mu} = 1.23$, corresponding to the best-fit value from the ML fit.

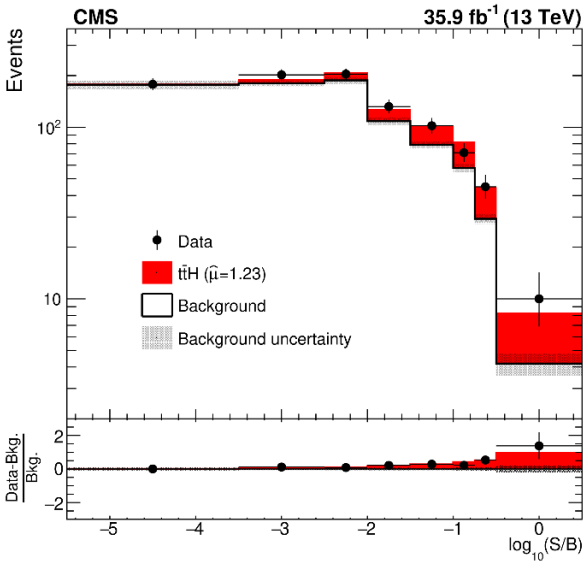

Figure 5. Distribution of the decimal logarithm of the ratio between the expected signal and expected background in each bin of the distributions used for the signal extraction. The distributions expected for signal and background processes are shown for the values of nuisance parameters obtained from the combined ML fit and $\mu = \hat{\mu} = 1.23$, corresponding to the best-fit value from the ML fit.

modes by $\mathrm{H} \to \mathrm{VV}$ and performing a two-parameter simultaneous fit for the signal rates $\mu(\mathrm{t\bar{t}H}, \mathrm{H} \to \mathrm{VV})$ and $\mu(\mathrm{t\bar{t}H}, \mathrm{H} \to \tau\tau)$, we obtain $\mu(\mathrm{t\bar{t}H}, \mathrm{H} \to \mathrm{VV}) = 1.69^{+0.68}_{-0.61}$ and $\mu(\mathrm{t\bar{t}H}, \mathrm{H} \to \tau\tau) = 0.15^{+1.07}_{-0.91}$. The expected anti-correlation between the two measured signal strengths has been explicitly checked and is associated with a correlation factor of -0.45.

As a cross check, the analysis is repeated with the $\mathrm{t\bar{t}Z}$ and $\mathrm{t\bar{t}W}(W)$ backgrounds kept freely floating in the ML fit. Control regions enriched in the contributions of these backgrounds are added to the fit to constrain them. The $\mathrm{t\bar{t}Z}$-enriched control region is defined from the 3ℓ signal region by inverting the Z boson veto on the invariant mass of SFOS lepton pairs. The $\mathrm{t\bar{t}W}$-enriched control region is defined from the $2\ell\mathrm{ss}$ signal region but changing the jet multiplicity requirement to consider events with exactly three jets. The signal rate obtained from this fit is $\mu = 1.04^{+0.50}_{-0.36}$ $(1.00^{+0.42}_{-0.38})$ times the SM $\mathrm{t\bar{t}H}$ production rate, with an observed (expected) significance of 2.7σ (2.7σ).

10 Summary

A search has been presented for the associated production of a Higgs boson with a top quark pair in final states with electrons, muons, and hadronically decaying τ leptons (τ_h). The analyzed data set corresponds to an integrated luminosity of $35.9\,\mathrm{fb}^{-1}$ of pp collision data recorded by the CMS experiment at $\sqrt{s} = 13\,\mathrm{TeV}$. The analysis is performed in six mutually exclusive event categories, based on different lepton and τ_h multiplicity requirements. The sensitivity of the analysis is enhanced by using multivariate analysis techniques based on

JHEP08(2018)066

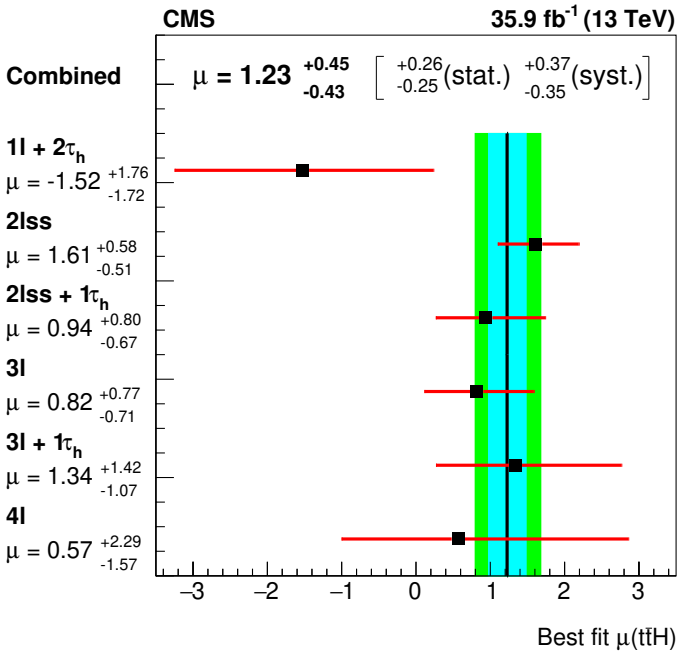

Figure 6. Signal rates μ, in units of the SM $\mathrm{t\bar{t}H}$ production rate, measured in each of the categories individually and for the combination of all six categories. The blue (green) band corresponds to the statistical (total) uncertainty on the combined signal rate.

boosted decision trees and on the matrix element method. The results of the analysis are in agreement with the standard model (SM) expectation. The measured signal rate amounts to $1.23^{+0.45}_{-0.43}$ times the SM $\mathrm{t\bar{t}H}$ production rate, with an observed (expected) significance of 3.2σ (2.8σ), which represents evidence for $\mathrm{t\bar{t}H}$ production in those final states. An upper limit on the signal rate of 2.1 times the SM $\mathrm{t\bar{t}H}$ production rate is set at 95% confidence level, for an expected limit of 1.7 times the SM production rate in the presence of a $\mathrm{t\bar{t}H}$ signal.

Acknowledgments

We congratulate our colleagues in the CERN accelerator departments for the excellent performance of the LHC and thank the technical and administrative staffs at CERN and at other CMS institutes for their contributions to the success of the CMS effort. In addition, we gratefully acknowledge the computing centers and personnel of the Worldwide LHC Computing Grid for delivering so effectively the computing infrastructure essential to our analyses. Finally, we acknowledge the enduring support for the construction and operation of the LHC and the CMS detector provided by the following funding agencies: BMWFW and FWF (Austria); FNRS and FWO (Belgium); CNPq, CAPES, FAPERJ, and FAPESP (Brazil); MES (Bulgaria); CERN; CAS, MoST, and NSFC (China); COLCIENCIAS (Colombia); MSES and CSF (Croatia); RPF (Cyprus); SENESCYT (Ecuador);

JHEP08(2018)066

MoER, ERC IUT, and ERDF (Estonia); Academy of Finland, MEC, and HIP (Finland); CEA and CNRS/IN2P3 (France); BMBF, DFG, and HGF (Germany); GSRT (Greece); NKFIA (Hungary); DAE and DST (India); IPM (Iran); SFI (Ireland); INFN (Italy); MSIP and NRF (Republic of Korea); LAS (Lithuania); MOE and UM (Malaysia); BUAP, CINVESTAV, CONACYT, LNS, SEP, and UASLP-FAI (Mexico); MBIE (New Zealand); PAEC (Pakistan); MSHE and NSC (Poland); FCT (Portugal); JINR (Dubna); MON, RosAtom, RAS, RFBR and RAEP (Russia); MESTD (Serbia); SEIDI, CPAN, PCTI and FEDER (Spain); Swiss Funding Agencies (Switzerland); MST (Taipei); ThEPCenter, IPST, STAR, and NSTDA (Thailand); TUBITAK and TAEK (Turkey); NASU and SFFR (Ukraine); STFC (United Kingdom); DOE and NSF (U.S.A.).

Individuals have received support from the Marie-Curie program and the European Research Council and Horizon 2020 Grant, contract No. 675440 (European Union); the Leventis Foundation; the A.P. Sloan Foundation; the Alexander von Humboldt Foundation; the Belgian Federal Science Policy Office; the Fonds pour la Formation à la Recherche dans l'Industrie et dans l'Agriculture (FRIA-Belgium); the Agentschap voor Innovatie door Wetenschap en Technologie (IWT-Belgium); the F.R.S.-FNRS and FWO (Belgium) under the "Excellence of Science — EOS" — be.h project n. 30820817; the Ministry of Education, Youth and Sports (MEYS) of the Czech Republic; the Lendület ("Momentum") Program and the János Bolyai Research Scholarship of the Hungarian Academy of Sciences, the New National Excellence Program ÚNKP, the NKFIA research grants 123842, 123959, 124845, 124850 and 125105 (Hungary); the Council of Science and Industrial Research, India; the HOMING PLUS program of the Foundation for Polish Science, cofinanced from European Union, Regional Development Fund, the Mobility Plus program of the Ministry of Science and Higher Education, the National Science Center (Poland), contracts Harmonia 2014/14/M/ST2/00428, Opus 2014/13/B/ST2/02543, 2014/15/B/ST2/03998, and 2015/19/B/ST2/02861, Sonata-bis 2012/07/E/ST2/01406; the National Priorities Research Program by Qatar National Research Fund; the Programa Estatal de Fomento de la Investigación Científica y Técnica de Excelencia María de Maeztu, grant MDM-2015-0509 and the Programa Severo Ochoa del Principado de Asturias; the Thalis and Aristeia programs cofinanced by EU-ESF and the Greek NSRF; the Rachadapisek Sompot Fund for Postdoctoral Fellowship, Chulalongkorn University and the Chulalongkorn Academic into Its 2nd Century Project Advancement Project (Thailand); the Welch Foundation, contract C-1845; and the Weston Havens Foundation (U.S.A.).

JHEP08(2018)066

A Matrix element method

As mentioned in section 7.1, discriminants based on the MEM approach have been developed for the $2\ell\mathrm{ss}+1\tau_\mathrm{h}$ and 3ℓ categories. Additional details on their computation are given in this appendix. The matrix element (ME) $\mathcal{M}_\Omega(\mathbf{x})$ associated with a given process Ω depends on a set of kinematic variables $\mathbf{x}$ that corresponds to the four-momenta, at parton level, of the particles in the initial and final state. We use bold letters to indicate vector quantities. The square of the ME is convoluted with a function $W(\mathbf{y}|\mathbf{x})$, referred to as the "transfer function" (TF), which represents the experimental resolution. More specifically,

the function $W(\mathbf{y}|\mathbf{x})$ corresponds to the probability for measuring a set of observables $\mathbf{y}$ in the detector, given that the corresponding parton-level momenta are equal to $\mathbf{x}$.

The MEM computes the differential cross section of the process Ω with respect to the observables $\mathbf{y}$, while integrating over the unmeasured or poorly measured parton-level quantities $\mathbf{x}$, as well as over the Bjorken scaling variables [72] x_a and x_b of the colliding protons. For each event a weight $w_\Omega(\mathbf{y})$ is computed, which quantifies the compatibility of the event, characterized by the measured observables $\mathbf{y}$, with the hypotheses that the event is produced by the process Ω:

$$w_\Omega(\mathbf{y}) \propto \sum_p \int \mathrm{d}\mathbf{x}\,\mathrm{d}x_a\,\mathrm{d}x_b \frac{f_i(x_a,Q) f_j(x_b,Q)}{x_a x_b s} \delta^4\left(x_a P_a + x_b P_b - \sum p_k\right) |\mathcal{M}_\Omega(\mathbf{x})|^2 W(\mathbf{y}|\mathbf{x}). \tag{A.1}$$

The sum $\sum_p$ extends over all possible associations between parton-level and reconstructed objects. The square of the ME, $|\mathcal{M}_\Omega(\mathbf{x})|^2$, is computed at LO using the MadGraph5_aMC@NLO program. The symbols $f_i(x_a, Q)$ and $f_j(x_b, Q)$ denote the PDFs, which we evaluate numerically using the CTEQ6.6 [73] and NNPDF3.0 LO sets. The four-dimensional δ-function $\delta^4(x_a P_a + x_b P_b - \sum p_k)$ ensures the conservation of energy and momentum. The integral on the right-hand side is first transformed analytically, in order to eliminate the δ-function and to make the computation of the integral numerically tractable, and then computed numerically using the VEGAS algorithm [74]. A complication arises from the fact that we use LO ME for the $\mathrm{t\bar{t}H}$ signal and for background processes. The LO ME strictly applies only to events in which no additional jets, besides the jets corresponding to quarks in the LO ME, are produced in the hard scattering interaction. At the center-of-mass energies of the LHC the phase space for quantum chromodynamics radiation is large, however, and particles with masses up to a few hundred GeV are typically produced in association with a sizable hadronic activity [75]. In order to use the LO ME, we transform the system of all particles that are present in the LO ME into a frame in which this system has zero p_T. In the opposite case of events where the reconstructed jet multiplicity is lower than the number of quarks present in the LO ME the integral on the right-hand-side of eq. (A.1) is extended by an integration over the variables associated to the missing jets. The TFs $W(\mathbf{y}|\mathbf{x})$ are obtained from the MC simulation and are used to model the p_T resolution of jets and the resolution on $\vec{p}_\mathrm{T}^{\,\mathrm{miss}}$. Separate TFs are used for b quark and for light quark and gluon jets. The TFs are also used to account for the energy loss due to neutrinos produced in the decays of b quarks to leptons and in τ lepton decays. The fraction of τ lepton energy carried by neutrinos is on average higher in $\tau \to \ell\overline{\nu}_\ell\nu_\tau$ decays compared to $\tau \to \tau_\mathrm{h}\nu_\tau$ decays and separate TFs are determined for both cases.

According to the Neyman lemma [76], the ratio of weights $w_\Omega(\mathbf{y})$ computed for the signal and for the background hypothesis constitutes an optimal observable to separate the $\mathrm{t\bar{t}H}$ signal from backgrounds:

$$\mathrm{LR}(\mathbf{y}) = \frac{w_{\mathrm{t\bar{t}H}}(\mathbf{y})}{w_{\mathrm{t\bar{t}H}}(\mathbf{y}) + \sum_\mathrm{B} \kappa_\mathrm{B}\, w_\mathrm{B}(\mathbf{y})}. \tag{A.2}$$

The coefficients κ_B that quantify the relative importance of different background processes

JHEP08(2018)066

B are determined by a numerical optimization, in order to achieve the maximal separation of the $t\bar{t}H$ signal from all background processes.

References

[1] ATLAS collaboration, *Observation of a new particle in the search for the Standard Model Higgs boson with the ATLAS detector at the LHC*, *Phys. Lett.* **B 716** (2012) 1 [arXiv:1207.7214] [INSPIRE].

[2] CMS collaboration, *Observation of a new boson at a mass of* 125 *GeV with the CMS experiment at the LHC*, *Phys. Lett.* **B 716** (2012) 30 [arXiv:1207.7235] [INSPIRE].

[3] CMS collaboration, *Observation of a new boson with mass near* 125 *GeV in pp collisions at* $\sqrt{s} = 7$ *and* 8 *TeV*, *JHEP* **06** (2013) 081 [arXiv:1303.4571] [INSPIRE].

[4] CMS collaboration, *Measurements of properties of the Higgs boson decaying into the four-lepton final state in pp collisions at* $\sqrt{s} = 13$ *TeV*, *JHEP* **11** (2017) 047 [arXiv:1706.09936] [INSPIRE].

[5] ATLAS collaboration, *Evidence for the spin-*0 *nature of the Higgs boson using ATLAS data*, *Phys. Lett.* **B 726** (2013) 120 [arXiv:1307.1432] [INSPIRE].

[6] CMS collaboration, *Constraints on the spin-parity and anomalous HVV couplings of the Higgs boson in proton collisions at* 7 *and* 8 *TeV*, *Phys. Rev.* **D 92** (2015) 012004 [arXiv:1411.3441] [INSPIRE].

[7] ATLAS collaboration, *Search for the Standard Model Higgs boson produced in association with top quarks and decaying into* $b\bar{b}$ *in pp collisions at* $\sqrt{s} = 8$ *TeV with the ATLAS detector*, *Eur. Phys. J.* **C 75** (2015) 349 [arXiv:1503.05066] [INSPIRE].

[8] ATLAS collaboration, *Search for the Standard Model Higgs boson decaying into* $b\bar{b}$ *produced in association with top quarks decaying hadronically in pp collisions at* $\sqrt{s} = 8$ *TeV with the ATLAS detector*, *JHEP* **05** (2016) 160 [arXiv:1604.03812] [INSPIRE].

[9] ATLAS collaboration, *Search for the associated production of the Higgs boson with a top quark pair in multilepton final states with the ATLAS detector*, *Phys. Lett.* **B 749** (2015) 519 [arXiv:1506.05988] [INSPIRE].

[10] ATLAS collaboration, *Search for* $H \to \gamma\gamma$ *produced in association with top quarks and constraints on the Yukawa coupling between the top quark and the Higgs boson using data taken at* 7 *TeV and* 8 *TeV with the ATLAS detector*, *Phys. Lett.* **B 740** (2015) 222 [arXiv:1409.3122] [INSPIRE].

[11] CMS collaboration, *Search for the associated production of the Higgs boson with a top-quark pair*, *JHEP* **09** (2014) 087 [*Erratum JHEP* **10** (2014) 106] [arXiv:1408.1682] [INSPIRE].

[12] CMS collaboration, *Search for a Standard Model Higgs Boson Produced in Association with a Top-Quark Pair and Decaying to Bottom Quarks Using a Matrix Element Method*, *Eur. Phys. J.* **C 75** (2015) 251 [arXiv:1502.02485] [INSPIRE].

[13] ATLAS collaboration, *Search for the standard model Higgs boson produced in association with top quarks and decaying into a* $b\bar{b}$ *pair in pp collisions at* $\sqrt{s} = 13$ *TeV with the ATLAS detector*, *Phys. Rev.* **D 97** (2018) 072016 [arXiv:1712.08895] [INSPIRE].

JHEP08(2018)066

[14] ATLAS collaboration, *Evidence for the associated production of the Higgs boson and a top quark pair with the ATLAS detector*, *Phys. Rev.* **D 97** (2018) 072003 [arXiv:1712.08891] [INSPIRE].

[15] A. Höcker, H. Voss, J. Stelzer and F. Tegenfeldt, *TMVA, the Toolkit for Multivariate Data Analysis with ROOT*, PoS(ACAT)040 [physics/0703039] [INSPIRE].

[16] F. Pedregosa et al., *Scikit-learn: Machine Learning in Python*, *J. Machine Learning Res.* **12** (2011) 2825 [arXiv:1201.0490] [INSPIRE].

[17] K. Kondo, *Dynamical Likelihood Method for Reconstruction of Events With Missing Momentum. 1: Method and Toy Models*, *J. Phys. Soc. Jap.* **57** (1988) 4126 [INSPIRE].

[18] K. Kondo, *Dynamical likelihood method for reconstruction of events with missing momentum. 2: Mass spectra for* $2 \to 2$ *processes*, *J. Phys. Soc. Jap.* **60** (1991) 836 [INSPIRE].

[19] CMS collaboration, *Description and performance of track and primary-vertex reconstruction with the CMS tracker*, 2014 *JINST* **9** P10009 [arXiv:1405.6569] [INSPIRE].

[20] CMS collaboration, *The CMS trigger system*, 2017 *JINST* **12** P01020 [arXiv:1609.02366] [INSPIRE].

[21] CMS collaboration, *The CMS Experiment at the CERN LHC*, 2008 *JINST* **3** S08004 [INSPIRE].

[22] J. Alwall et al., *The automated computation of tree-level and next-to-leading order differential cross sections and their matching to parton shower simulations*, *JHEP* **07** (2014) 079 [arXiv:1405.0301] [INSPIRE].

[23] J. Alwall et al., *Comparative study of various algorithms for the merging of parton showers and matrix elements in hadronic collisions*, *Eur. Phys. J.* **C 53** (2008) 473 [arXiv:0706.2569] [INSPIRE].

[24] P. Artoisenet, R. Frederix, O. Mattelaer and R. Rietkerk, *Automatic spin-entangled decays of heavy resonances in Monte Carlo simulations*, *JHEP* **03** (2013) 015 [arXiv:1212.3460] [INSPIRE].

[25] R. Frederix and S. Frixione, *Merging meets matching in MC@NLO*, *JHEP* **12** (2012) 061 [arXiv:1209.6215] [INSPIRE].

[26] P. Nason, *A New method for combining NLO QCD with shower Monte Carlo algorithms*, *JHEP* **11** (2004) 040 [hep-ph/0409146] [INSPIRE].

[27] S. Frixione, P. Nason and C. Oleari, *Matching NLO QCD computations with Parton Shower simulations: the POWHEG method*, *JHEP* **11** (2007) 070 [arXiv:0709.2092] [INSPIRE].

[28] S. Alioli, P. Nason, C. Oleari and E. Re, *A general framework for implementing NLO calculations in shower Monte Carlo programs: the POWHEG BOX*, *JHEP* **06** (2010) 043 [arXiv:1002.2581] [INSPIRE].

[29] NNPDF collaboration, R.D. Ball et al., *Parton distributions with QED corrections*, *Nucl. Phys.* **B 877** (2013) 290 [arXiv:1308.0598] [INSPIRE].

[30] NNPDF collaboration, R.D. Ball et al., *Unbiased global determination of parton distributions and their uncertainties at NNLO and at LO*, *Nucl. Phys.* **B 855** (2012) 153 [arXiv:1107.2652] [INSPIRE].

[31] NNPDF collaboration, R.D. Ball et al., *Parton distributions for the LHC Run II*, *JHEP* **04** (2015) 040 [arXiv:1410.8849] [INSPIRE].

JHEP08(2018)066

[32] T. Sjöstrand, S. Mrenna and P.Z. Skands, *A Brief Introduction to PYTHIA 8.1*, *Comput. Phys. Commun.* **178** (2008) 852 [arXiv:0710.3820] [INSPIRE].

[33] CMS collaboration, *Event generator tunes obtained from underlying event and multiparton scattering measurements*, *Eur. Phys. J.* **C 76** (2016) 155 [arXiv:1512.00815] [INSPIRE].

[34] Y. Li and F. Petriello, *Combining QCD and electroweak corrections to dilepton production in FEWZ*, *Phys. Rev.* **D 86** (2012) 094034 [arXiv:1208.5967] [INSPIRE].

[35] M. Czakon and A. Mitov, *Top++: A Program for the Calculation of the Top-Pair Cross-Section at Hadron Colliders*, *Comput. Phys. Commun.* **185** (2014) 2930 [arXiv:1112.5675] [INSPIRE].

[36] P. Kant et al., *HatHor for single top-quark production: Updated predictions and uncertainty estimates for single top-quark production in hadronic collisions*, *Comput. Phys. Commun.* **191** (2015) 74 [arXiv:1406.4403] [INSPIRE].

[37] M. Aliev, H. Lacker, U. Langenfeld, S. Moch, P. Uwer and M. Wiedermann, *HATHOR: HAdronic Top and Heavy quarks crOss section calculatoR*, *Comput. Phys. Commun.* **182** (2011) 1034 [arXiv:1007.1327] [INSPIRE].

[38] N. Kidonakis, *Two-loop soft anomalous dimensions for single top quark associated production with a W^- or H^-*, *Phys. Rev.* **D 82** (2010) 054018 [arXiv:1005.4451] [INSPIRE].

[39] J.M. Campbell, R.K. Ellis and C. Williams, *Vector boson pair production at the LHC*, *JHEP* **07** (2011) 018 [arXiv:1105.0020] [INSPIRE].

[40] GEANT4 collaboration, S. Agostinelli et al., *GEANT4: A Simulation toolkit*, *Nucl. Instrum. Meth.* **A 506** (2003) 250 [INSPIRE].

[41] CMS collaboration, *Performance of reconstruction and identification of tau leptons in their decays to hadrons and tau neutrino in LHC Run-2*, CMS-PAS-TAU-16-002 (2016) [INSPIRE].

[42] CMS collaboration, *Identification of b-quark jets with the CMS experiment*, 2013 *JINST* **8** P04013 [arXiv:1211.4462] [INSPIRE].

[43] CMS collaboration, *Performance of missing energy reconstruction in* 13 *TeV pp collision data using the CMS detector*, CMS-PAS-JME-16-004 (2016) [INSPIRE].

[44] CMS collaboration, *Performance of the CMS missing transverse momentum reconstruction in pp data at $\sqrt{s} = 8$ TeV*, 2015 *JINST* **10** P02006 [arXiv:1411.0511] [INSPIRE].

[45] CMS collaboration, *Particle-flow reconstruction and global event description with the CMS detector*, 2017 *JINST* **12** P10003 [arXiv:1706.04965] [INSPIRE].

[46] E. Chabanat and N. Estre, *Deterministic annealing for vertex finding at CMS*, in proceedings of the *14th International Conference on Computing in High-Energy and Nuclear Physics (CHEP 2004)*, Interlaken, Switzerland, 27 September–1 October 2004, pp. 287–290 [https://doi.org/10.5170/CERN-2005-002.287] [INSPIRE] and online pdf version at http://doc.cern.ch/yellowrep/2005/2005-002/p287.pdf.

[47] W. Waltenberger, R. Frühwirth and P. Vanlaer, *Adaptive vertex fitting*, *J. Phys.* **G 34** (2007) N343 [INSPIRE].

[48] M. Cacciari, G.P. Salam and G. Soyez, *The anti-k_t jet clustering algorithm*, *JHEP* **04** (2008) 063 [arXiv:0802.1189] [INSPIRE].

[49] M. Cacciari, G.P. Salam and G. Soyez, *FastJet User Manual*, *Eur. Phys. J.* **C 72** (2012) 1896 [arXiv:1111.6097] [INSPIRE].

JHEP08(2018)066

[50] CMS collaboration, *Performance of Electron Reconstruction and Selection with the CMS Detector in Proton-Proton Collisions at* $\sqrt{s} = 8$ *TeV*, 2015 *JINST* **10** P06005 [arXiv:1502.02701] [INSPIRE].

[51] CMS collaboration, *Performance of CMS muon reconstruction in pp collision events at* $\sqrt{s} = 7$ *TeV*, 2012 *JINST* **7** P10002 [arXiv:1206.4071] [INSPIRE].

[52] M. Cacciari, G.P. Salam and G. Soyez, *The Catchment Area of Jets*, *JHEP* **04** (2008) 005 [arXiv:0802.1188] [INSPIRE].

[53] M. Cacciari and G.P. Salam, *Pileup subtraction using jet areas*, *Phys. Lett.* **B 659** (2008) 119 [arXiv:0707.1378] [INSPIRE].

[54] CMS collaboration, *Reconstruction and identification of* τ *lepton decays to hadrons and* ν_τ *at CMS*, 2016 *JINST* **11** P01019 [arXiv:1510.07488] [INSPIRE].

[55] CMS collaboration, *Jet algorithms performance in* 13 *TeV data*, CMS-PAS-JME-16-003 (2017) [INSPIRE].

[56] CMS collaboration, *Determination of Jet Energy Calibration and Transverse Momentum Resolution in CMS*, 2011 *JINST* **6** P11002 [arXiv:1107.4277] [INSPIRE].

[57] CMS collaboration, *Identification of b quark jets at the CMS Experiment in the LHC Run 2*, CMS-PAS-BTV-15-001 (2016) [INSPIRE].

[58] J. MacQueen, *Some methods for classification and analysis of multivariate observations*, in proceedings of the *Fifth Berkeley Symposium on Mathematical Statistics and Probability*, Statistical Laboratory of the University of California, Berkeley, California, U.S.A., 21 June–18 July 1965 and 27 December 1965–7 January 1966, University of California Press, Berkeley California U.S.A. (1967), p. 281.

[59] ATLAS and CMS collaborations and The LHC Higgs Combination Group, *Procedure for the LHC Higgs boson search combination in Summer 2011*, ATL-PHYS-PUB-2011-011 (2011) [INSPIRE].

[60] CMS collaboration, *Combined results of searches for the standard model Higgs boson in pp collisions at* $\sqrt{s} = 7$ *TeV*, *Phys. Lett.* **B 710** (2012) 26 [arXiv:1202.1488] [INSPIRE].

[61] T. Junk, *Confidence level computation for combining searches with small statistics*, *Nucl. Instrum. Meth.* **A 434** (1999) 435 [hep-ex/9902006] [INSPIRE].

[62] A.L. Read, *Presentation of search results: The* CL_s *technique*, *J. Phys.* **G 28** (2002) 2693 [INSPIRE].

[63] J.S. Conway, *Incorporating Nuisance Parameters in Likelihoods for Multisource Spectra*, in proceedings of *PHYSTAT 2011*, Geneva, Switzerland, 17–20 January 2011, pp. 115–120 [https://doi.org/10.5170/CERN-2011-006.115] [arXiv:1103.0354] [INSPIRE].

[64] CMS collaboration, *Measurements of Inclusive W and Z Cross Sections in pp Collisions at* $\sqrt{s} = 7$ *TeV*, *JHEP* **01** (2011) 080 [arXiv:1012.2466] [INSPIRE].

[65] CMS collaboration, *CMS Luminosity Measurements for the 2016 Data Taking Period*, CMS-PAS-LUM-17-001 (2017) [INSPIRE].

[66] LHC Higgs Cross Section Working Group, D. de Florian et al., *Handbook of LHC Higgs Cross Sections: 4. Deciphering the Nature of the Higgs Sector*, arXiv:1610.07922 [INSPIRE].

[67] M. Cacciari, S. Frixione, M.L. Mangano, P. Nason and G. Ridolfi, *The* $t\bar{t}$ *cross-section at* 1.8 *TeV and* 1.96 *TeV: A Study of the systematics due to parton densities and scale dependence*, *JHEP* **04** (2004) 068 [hep-ph/0303085] [INSPIRE].

JHEP08(2018)066

[68] S. Catani, D. de Florian, M. Grazzini and P. Nason, *Soft gluon resummation for Higgs boson production at hadron colliders*, *JHEP* **07** (2003) 028 [hep-ph/0306211] [INSPIRE].

[69] R. Frederix, S. Frixione, V. Hirschi, F. Maltoni, R. Pittau and P. Torrielli, *Four-lepton production at hadron colliders: aMC@NLO predictions with theoretical uncertainties*, *JHEP* **02** (2012) 099 [arXiv:1110.4738] [INSPIRE].

[70] ATLAS collaboration, *Measurement of the $W^{\pm}Z$ boson pair-production cross section in pp collisions at $\sqrt{s} = 13$ TeV with the ATLAS Detector*, *Phys. Lett.* **B 762** (2016) 1 [arXiv:1606.04017] [INSPIRE].

[71] CMS collaboration, *Measurement of the WZ production cross section in pp collisions at $\sqrt{s} = 13$ TeV*, *Phys. Lett.* **B 766** (2017) 268 [arXiv:1607.06943] [INSPIRE].

[72] J.D. Bjorken, *Asymptotic Sum Rules at Infinite Momentum*, *Phys. Rev.* **179** (1969) 1547 [INSPIRE].

[73] P.M. Nadolsky et al., *Implications of CTEQ global analysis for collider observables*, *Phys. Rev.* **D 78** (2008) 013004 [arXiv:0802.0007] [INSPIRE].

[74] G.P. Lepage, *A New Algorithm for Adaptive Multidimensional Integration*, *J. Comput. Phys.* **27** (1978) 192 [INSPIRE].

[75] J. Alwall, A. Freitas and O. Mattelaer, *The Matrix Element Method and QCD Radiation*, *Phys. Rev.* **D 83** (2011) 074010 [arXiv:1010.2263] [INSPIRE].

[76] J. Neyman, *Outline of a theory of statistical estimation based on the classical theory of probability*, *Phil. Trans. Roy. Soc. Lond.* **A 236** (1937) 333 [INSPIRE].

JHEP08(2018)066

The CMS collaboration

Yerevan Physics Institute, Yerevan, Armenia

A.M. Sirunyan, A. Tumasyan

Institut für Hochenergiephysik, Wien, Austria

W. Adam, F. Ambrogi, E. Asilar, T. Bergauer, J. Brandstetter, E. Brondolin, M. Dragicevic, J. Erö, A. Escalante Del Valle, M. Flechl, M. Friedl, R. Frühwirth[1], V.M. Ghete, J. Grossmann, J. Hrubec, M. Jeitler[1], A. König, N. Krammer, I. Krätschmer, D. Liko, T. Madlener, I. Mikulec, E. Pree, N. Rad, H. Rohringer, J. Schieck[1], R. Schöfbeck, M. Spanring, D. Spitzbart, A. Taurok, W. Waltenberger, J. Wittmann, C.-E. Wulz[1], M. Zarucki

Institute for Nuclear Problems, Minsk, Belarus

V. Chekhovsky, V. Mossolov, J. Suarez Gonzalez

Universiteit Antwerpen, Antwerpen, Belgium

E.A. De Wolf, D. Di Croce, X. Janssen, J. Lauwers, M. Pieters, M. Van De Klundert, H. Van Haevermaet, P. Van Mechelen, N. Van Remortel

Vrije Universiteit Brussel, Brussel, Belgium

S. Abu Zeid, F. Blekman, J. D'Hondt, I. De Bruyn, J. De Clercq, K. Deroover, G. Flouris, D. Lontkovskyi, S. Lowette, I. Marchesini, S. Moortgat, L. Moreels, Q. Python, K. Skovpen, S. Tavernier, W. Van Doninck, P. Van Mulders, I. Van Parijs

Université Libre de Bruxelles, Bruxelles, Belgium

D. Beghin, B. Bilin, H. Brun, B. Clerbaux, G. De Lentdecker, H. Delannoy, B. Dorney, G. Fasanella, L. Favart, R. Goldouzian, A. Grebenyuk, A.K. Kalsi, T. Lenzi, J. Luetic, T. Seva, E. Starling, C. Vander Velde, P. Vanlaer, D. Vannerom, R. Yonamine

Ghent University, Ghent, Belgium

T. Cornelis, D. Dobur, A. Fagot, M. Gul, I. Khvastunov[2], D. Poyraz, C. Roskas, D. Trocino, M. Tytgat, W. Verbeke, B. Vermassen, M. Vit, N. Zaganidis

Université Catholique de Louvain, Louvain-la-Neuve, Belgium

H. Bakhshiansohi, O. Bondu, S. Brochet, G. Bruno, C. Caputo, A. Caudron, P. David, S. De Visscher, C. Delaere, M. Delcourt, B. Francois, A. Giammanco, G. Krintiras, V. Lemaitre, A. Magitteri, A. Mertens, M. Musich, K. Piotrzkowski, L. Quertenmont, A. Saggio, M. Vidal Marono, S. Wertz, J. Zobec

Centro Brasileiro de Pesquisas Fisicas, Rio de Janeiro, Brazil

W.L. Aldá Júnior, F.L. Alves, G.A. Alves, L. Brito, G. Correia Silva, C. Hensel, A. Moraes, M.E. Pol, P. Rebello Teles

Universidade do Estado do Rio de Janeiro, Rio de Janeiro, Brazil

E. Belchior Batista Das Chagas, W. Carvalho, J. Chinellato[3], E. Coelho, E.M. Da Costa, G.G. Da Silveira[4], D. De Jesus Damiao, S. Fonseca De Souza, H. Malbouisson, M. Medina Jaime[5], M. Melo De Almeida, C. Mora Herrera, L. Mundim, H. Nogima,

JHEP08(2018)066

L.J. Sanchez Rosas, A. Santoro, A. Sznajder, M. Thiel, E.J. Tonelli Manganote[3], F. Torres Da Silva De Araujo, A. Vilela Pereira

Universidade Estadual Paulista [a], Universidade Federal do ABC [b], São Paulo, Brazil

S. Ahuja[a], C.A. Bernardes[a], L. Calligaris[a], T.R. Fernandez Perez Tomei[a], E.M. Gregores[b], P.G. Mercadante[b], S.F. Novaes[a], Sandra S. Padula[a], D. Romero Abad[b], J.C. Ruiz Vargas[a]

Institute for Nuclear Research and Nuclear Energy, Bulgarian Academy of Sciences, Sofia, Bulgaria

A. Aleksandrov, R. Hadjiiska, P. Iaydjiev, A. Marinov, M. Misheva, M. Rodozov, M. Shopova, G. Sultanov

University of Sofia, Sofia, Bulgaria

A. Dimitrov, L. Litov, B. Pavlov, P. Petkov

Beihang University, Beijing, China

W. Fang[6], X. Gao[6], L. Yuan

Institute of High Energy Physics, Beijing, China

M. Ahmad, J.G. Bian, G.M. Chen, H.S. Chen, M. Chen, Y. Chen, C.H. Jiang, D. Leggat, B. Li, H. Liao, Z. Liu, F. Romeo, S.M. Shaheen, A. Spiezia, J. Tao, C. Wang, Z. Wang, E. Yazgan, H. Zhang, J. Zhao

State Key Laboratory of Nuclear Physics and Technology, Peking University, Beijing, China

Y. Ban, G. Chen, J. Li, Q. Li, S. Liu, Y. Mao, S.J. Qian, D. Wang, Z. Xu

Tsinghua University, Beijing, China

Y. Wang

Universidad de Los Andes, Bogota, Colombia

C. Avila, A. Cabrera, C.A. Carrillo Montoya, L.F. Chaparro Sierra, C. Florez, C.F. González Hernández, M.A. Segura Delgado

University of Split, Faculty of Electrical Engineering, Mechanical Engineering and Naval Architecture, Split, Croatia

B. Courbon, N. Godinovic, D. Lelas, I. Puljak, P.M. Ribeiro Cipriano, T. Sculac

University of Split, Faculty of Science, Split, Croatia

Z. Antunovic, M. Kovac

Institute Rudjer Boskovic, Zagreb, Croatia

V. Brigljevic, D. Ferencek, K. Kadija, B. Mesic, A. Starodumov[7], T. Susa

University of Cyprus, Nicosia, Cyprus

M.W. Ather, A. Attikis, G. Mavromanolakis, J. Mousa, C. Nicolaou, F. Ptochos, P.A. Razis, H. Rykaczewski

Charles University, Prague, Czech Republic

M. Finger[8], M. Finger Jr.[8]

JHEP08(2018)066

Universidad San Francisco de Quito, Quito, Ecuador
E. Carrera Jarrin

Academy of Scientific Research and Technology of the Arab Republic of Egypt, Egyptian Network of High Energy Physics, Cairo, Egypt
H. Abdalla[9], Y. Assran[10,11], A. Mohamed[12]

National Institute of Chemical Physics and Biophysics, Tallinn, Estonia
S. Bhowmik, R.K. Dewanjee, M. Kadastik, L. Perrini, M. Raidal, C. Veelken

Department of Physics, University of Helsinki, Helsinki, Finland
P. Eerola, H. Kirschenmann, J. Pekkanen, M. Voutilainen

Helsinki Institute of Physics, Helsinki, Finland
J. Havukainen, J.K. Heikkilä, T. Järvinen, V. Karimäki, R. Kinnunen, T. Lampén, K. Lassila-Perini, S. Laurila, S. Lehti, T. Lindén, P. Luukka, T. Mäenpää, H. Siikonen, E. Tuominen, J. Tuominiemi

Lappeenranta University of Technology, Lappeenranta, Finland
T. Tuuva

IRFU, CEA, Université Paris-Saclay, Gif-sur-Yvette, France
M. Besancon, F. Couderc, M. Dejardin, D. Denegri, J.L. Faure, F. Ferri, S. Ganjour, S. Ghosh, A. Givernaud, P. Gras, G. Hamel de Monchenault, P. Jarry, C. Leloup, E. Locci, M. Machet, J. Malcles, G. Negro, J. Rander, A. Rosowsky, M.Ö. Sahin, M. Titov

Laboratoire Leprince-Ringuet, Ecole polytechnique, CNRS/IN2P3, Université Paris-Saclay, Palaiseau, France
A. Abdulsalam[13], C. Amendola, I. Antropov, S. Baffioni, F. Beaudette, P. Busson, L. Cadamuro, C. Charlot, R. Granier de Cassagnac, M. Jo, I. Kucher, S. Lisniak, A. Lobanov, J. Martin Blanco, M. Nguyen, C. Ochando, G. Ortona, P. Paganini, P. Pigard, R. Salerno, J.B. Sauvan, Y. Sirois, A.G. Stahl Leiton, Y. Yilmaz, A. Zabi, A. Zghiche

Université de Strasbourg, CNRS, IPHC UMR 7178, F-67000 Strasbourg, France
J.-L. Agram[14], J. Andrea, D. Bloch, J.-M. Brom, M. Buttignol, E.C. Chabert, C. Collard, E. Conte[14], X. Coubez, F. Drouhin[14], J.-C. Fontaine[14], D. Gelé, U. Goerlach, M. Jansová, P. Juillot, A.-C. Le Bihan, N. Tonon, P. Van Hove

Centre de Calcul de l'Institut National de Physique Nucleaire et de Physique des Particules, CNRS/IN2P3, Villeurbanne, France
S. Gadrat

Université de Lyon, Université Claude Bernard Lyon 1, CNRS-IN2P3, Institut de Physique Nucléaire de Lyon, Villeurbanne, France
S. Beauceron, C. Bernet, G. Boudoul, N. Chanon, R. Chierici, D. Contardo, P. Depasse, H. El Mamouni, J. Fay, L. Finco, S. Gascon, M. Gouzevitch, G. Grenier, B. Ille, F. Lagarde, I.B. Laktineh, H. Lattaud, M. Lethuillier, L. Mirabito, A.L. Pequegnot, S. Perries, A. Popov[15], V. Sordini, M. Vander Donckt, S. Viret, S. Zhang

JHEP08(2018)066

Georgian Technical University, Tbilisi, Georgia

A. Khvedelidze[8]

Tbilisi State University, Tbilisi, Georgia

Z. Tsamalaidze[8]

RWTH Aachen University, I. Physikalisches Institut, Aachen, Germany

C. Autermann, L. Feld, M.K. Kiesel, K. Klein, M. Lipinski, M. Preuten, M.P. Rauch, C. Schomakers, J. Schulz, M. Teroerde, B. Wittmer, V. Zhukov[15]

RWTH Aachen University, III. Physikalisches Institut A, Aachen, Germany

A. Albert, D. Duchardt, M. Endres, M. Erdmann, S. Erdweg, T. Esch, R. Fischer, A. Güth, T. Hebbeker, C. Heidemann, K. Hoepfner, S. Knutzen, M. Merschmeyer, A. Meyer, P. Millet, S. Mukherjee, T. Pook, M. Radziej, H. Reithler, M. Rieger, F. Scheuch, D. Teyssier, S. Thüer

RWTH Aachen University, III. Physikalisches Institut B, Aachen, Germany

G. Flügge, B. Kargoll, T. Kress, A. Künsken, T. Müller, A. Nehrkorn, A. Nowack, C. Pistone, O. Pooth, A. Stahl[16]

Deutsches Elektronen-Synchrotron, Hamburg, Germany

M. Aldaya Martin, T. Arndt, C. Asawatangtrakuldee, K. Beernaert, O. Behnke, U. Behrens, A. Bermúdez Martínez, A.A. Bin Anuar, K. Borras[17], V. Botta, A. Campbell, P. Connor, C. Contreras-Campana, F. Costanza, V. Danilov, A. De Wit, C. Diez Pardos, D. Domínguez Damiani, G. Eckerlin, D. Eckstein, T. Eichhorn, E. Eren, E. Gallo[18], J. Garay Garcia, A. Geiser, J.M. Grados Luyando, A. Grohsjean, P. Gunnellini, M. Guthoff, A. Harb, J. Hauk, M. Hempel[19], H. Jung, M. Kasemann, J. Keaveney, C. Kleinwort, J. Knolle, I. Korol, D. Krücker, W. Lange, A. Lelek, T. Lenz, K. Lipka, W. Lohmann[19], R. Mankel, I.-A. Melzer-Pellmann, A.B. Meyer, M. Meyer, M. Missiroli, G. Mittag, J. Mnich, A. Mussgiller, D. Pitzl, A. Raspereza, M. Savitskyi, P. Saxena, R. Shevchenko, N. Stefaniuk, H. Tholen, G.P. Van Onsem, R. Walsh, Y. Wen, K. Wichmann, C. Wissing, O. Zenaiev

University of Hamburg, Hamburg, Germany

R. Aggleton, S. Bein, V. Blobel, M. Centis Vignali, T. Dreyer, E. Garutti, D. Gonzalez, J. Haller, A. Hinzmann, M. Hoffmann, A. Karavdina, G. Kasieczka, R. Klanner, R. Kogler, N. Kovalchuk, S. Kurz, D. Marconi, J. Multhaup, M. Niedziela, D. Nowatschin, T. Peiffer, A. Perieanu, A. Reimers, C. Scharf, P. Schleper, A. Schmidt, S. Schumann, J. Schwandt, J. Sonneveld, H. Stadie, G. Steinbrück, F.M. Stober, M. Stöver, D. Troendle, E. Usai, A. Vanhoefer, B. Vormwald

Institut für Experimentelle Teilchenphysik, Karlsruhe, Germany

M. Akbiyik, C. Barth, M. Baselga, S. Baur, E. Butz, R. Caspart, T. Chwalek, F. Colombo, W. De Boer, A. Dierlamm, N. Faltermann, B. Freund, R. Friese, M. Giffels, M.A. Harrendorf, F. Hartmann[16], S.M. Heindl, U. Husemann, F. Kassel[16], S. Kudella, H. Mildner, M.U. Mozer, Th. Müller, M. Plagge, G. Quast, K. Rabbertz, M. Schröder, I. Shvetsov,

JHEP08(2018)066

G. Sieber, H.J. Simonis, R. Ulrich, S. Wayand, M. Weber, T. Weiler, S. Williamson, C. Wöhrmann, R. Wolf

Institute of Nuclear and Particle Physics (INPP), NCSR Demokritos, Aghia Paraskevi, Greece

G. Anagnostou, G. Daskalakis, T. Geralis, A. Kyriakis, D. Loukas, I. Topsis-Giotis

National and Kapodistrian University of Athens, Athens, Greece

G. Karathanasis, S. Kesisoglou, A. Panagiotou, N. Saoulidou, E. Tziaferi

National Technical University of Athens, Athens, Greece

K. Kousouris, I. Papakrivopoulos

University of Ioánnina, Ioánnina, Greece

I. Evangelou, C. Foudas, P. Gianneios, P. Katsoulis, P. Kokkas, S. Mallios, N. Manthos, I. Papadopoulos, E. Paradas, J. Strologas, F.A. Triantis, D. Tsitsonis

MTA-ELTE Lendület CMS Particle and Nuclear Physics Group, Eötvös Loránd University, Budapest, Hungary

M. Csanad, N. Filipovic, G. Pasztor, O. Surányi, G.I. Veres[20]

Wigner Research Centre for Physics, Budapest, Hungary

G. Bencze, C. Hajdu, D. Horvath[21], Á. Hunyadi, F. Sikler, T.Á. Vámi, V. Veszpremi, G. Vesztergombi[20]

Institute of Nuclear Research ATOMKI, Debrecen, Hungary

N. Beni, S. Czellar, J. Karancsi[22], A. Makovec, J. Molnar, Z. Szillasi

Institute of Physics, University of Debrecen, Debrecen, Hungary

M. Bartók[20], P. Raics, Z.L. Trocsanyi, B. Ujvari

Indian Institute of Science (IISc), Bangalore, India

S. Choudhury, J.R. Komaragiri

National Institute of Science Education and Research, Bhubaneswar, India

S. Bahinipati[23], P. Mal, K. Mandal, A. Nayak[24], D.K. Sahoo[23], S.K. Swain

Panjab University, Chandigarh, India

S. Bansal, S.B. Beri, V. Bhatnagar, S. Chauhan, R. Chawla, N. Dhingra, R. Gupta, A. Kaur, M. Kaur, S. Kaur, R. Kumar, P. Kumari, M. Lohan, A. Mehta, S. Sharma, J.B. Singh, G. Walia

University of Delhi, Delhi, India

A. Bhardwaj, B.C. Choudhary, R.B. Garg, S. Keshri, A. Kumar, Ashok Kumar, S. Malhotra, M. Naimuddin, K. Ranjan, Aashaq Shah, R. Sharma

Saha Institute of Nuclear Physics, HBNI, Kolkata, India

R. Bhardwaj[25], R. Bhattacharya, S. Bhattacharya, U. Bhawandeep[25], D. Bhowmik, S. Dey, S. Dutt[25], S. Dutta, S. Ghosh, N. Majumdar, K. Mondal, S. Mukhopadhyay, S. Nandan, A. Purohit, P.K. Rout, A. Roy, S. Roy Chowdhury, S. Sarkar, M. Sharan, B. Singh, S. Thakur[25]

JHEP08(2018)066

Indian Institute of Technology Madras, Madras, India
P.K. Behera

Bhabha Atomic Research Centre, Mumbai, India
R. Chudasama, D. Dutta, V. Jha, V. Kumar, A.K. Mohanty[16], P.K. Netrakanti, L.M. Pant, P. Shukla, A. Topkar

Tata Institute of Fundamental Research-A, Mumbai, India
T. Aziz, S. Dugad, B. Mahakud, S. Mitra, G.B. Mohanty, N. Sur, B. Sutar

Tata Institute of Fundamental Research-B, Mumbai, India
S. Banerjee, S. Bhattacharya, S. Chatterjee, P. Das, M. Guchait, Sa. Jain, S. Kumar, M. Maity[26], G. Majumder, K. Mazumdar, N. Sahoo, T. Sarkar[26], N. Wickramage[27]

Indian Institute of Science Education and Research (IISER), Pune, India
S. Chauhan, S. Dube, V. Hegde, A. Kapoor, K. Kothekar, S. Pandey, A. Rane, S. Sharma

Institute for Research in Fundamental Sciences (IPM), Tehran, Iran
S. Chenarani[28], E. Eskandari Tadavani, S.M. Etesami[28], M. Khakzad, M. Mohammadi Najafabadi, M. Naseri, S. Paktinat Mehdiabadi[29], F. Rezaei Hosseinabadi, B. Safarzadeh[30], M. Zeinali

University College Dublin, Dublin, Ireland
M. Felcini, M. Grunewald

INFN Sezione di Bari [a], Università di Bari [b], Politecnico di Bari [c], Bari, Italy
M. Abbrescia[a,b], C. Calabria[a,b], A. Colaleo[a], D. Creanza[a,c], L. Cristella[a,b], N. De Filippis[a,c], M. De Palma[a,b], A. Di Florio[a,b], F. Errico[a,b], L. Fiore[a], A. Gelmi[a,b], G. Iaselli[a,c], S. Lezki[a,b], G. Maggi[a,c], M. Maggi[a], B. Marangelli[a,b], G. Miniello[a,b], S. My[a,b], S. Nuzzo[a,b], A. Pompili[a,b], G. Pugliese[a,c], R. Radogna[a], A. Ranieri[a], G. Selvaggi[a,b], A. Sharma[a], L. Silvestris[a,16], R. Venditti[a], P. Verwilligen[a], G. Zito[a]

INFN Sezione di Bologna [a], Università di Bologna [b], Bologna, Italy
G. Abbiendi[a], C. Battilana[a,b], D. Bonacorsi[a,b], L. Borgonovi[a,b], S. Braibant-Giacomelli[a,b], R. Campanini[a,b], P. Capiluppi[a,b], A. Castro[a,b], F.R. Cavallo[a], S.S. Chhibra[a,b], G. Codispoti[a,b], M. Cuffiani[a,b], G.M. Dallavalle[a], F. Fabbri[a], A. Fanfani[a,b], D. Fasanella[a,b], P. Giacomelli[a], C. Grandi[a], L. Guiducci[a,b], S. Marcellini[a], G. Masetti[a], A. Montanari[a], F.L. Navarria[a,b], F. Odorici[a], A. Perrotta[a], A.M. Rossi[a,b], T. Rovelli[a,b], G.P. Siroli[a,b], N. Tosi[a]

INFN Sezione di Catania [a], Università di Catania [b], Catania, Italy
S. Albergo[a,b], S. Costa[a,b], A. Di Mattia[a], F. Giordano[a,b], R. Potenza[a,b], A. Tricomi[a,b], C. Tuve[a,b]

INFN Sezione di Firenze [a], Università di Firenze [b], Firenze, Italy
G. Barbagli[a], K. Chatterjee[a,b], V. Ciulli[a,b], C. Civinini[a], R. D'Alessandro[a,b], E. Focardi[a,b], G. Latino, P. Lenzi[a,b], M. Meschini[a], S. Paoletti[a], L. Russo[a,31], G. Sguazzoni[a], D. Strom[a], L. Viliani[a]

JHEP08(2018)066

INFN Laboratori Nazionali di Frascati, Frascati, Italy

L. Benussi, S. Bianco, F. Fabbri, D. Piccolo, F. Primavera[16]

INFN Sezione di Genova [a], Università di Genova [b], Genova, Italy

V. Calvelli[a,b], F. Ferro[a], F. Ravera[a,b], E. Robutti[a], S. Tosi[a,b]

INFN Sezione di Milano-Bicocca [a], Università di Milano-Bicocca [b], Milano, Italy

A. Benaglia[a], A. Beschi[b], L. Brianza[a,b], F. Brivio[a,b], V. Ciriolo[a,b,16], M.E. Dinardo[a,b], S. Fiorendi[a,b], S. Gennai[a], A. Ghezzi[a,b], P. Govoni[a,b], M. Malberti[a,b], S. Malvezzi[a], R.A. Manzoni[a,b], D. Menasce[a], L. Moroni[a], M. Paganoni[a,b], K. Pauwels[a,b], D. Pedrini[a], S. Pigazzini[a,b,32], S. Ragazzi[a,b], T. Tabarelli de Fatis[a,b]

INFN Sezione di Napoli [a], Università di Napoli 'Federico II' [b], Napoli, Italy, Università della Basilicata [c], Potenza, Italy, Università G. Marconi [d], Roma, Italy

S. Buontempo[a], N. Cavallo[a,c], S. Di Guida[a,d,16], F. Fabozzi[a,c], F. Fienga[a,b], G. Galati[a,b], A.O.M. Iorio[a,b], W.A. Khan[a], L. Lista[a], S. Meola[a,d,16], P. Paolucci[a,16], C. Sciacca[a,b], F. Thyssen[a], E. Voevodina[a,b]

INFN Sezione di Padova [a], Università di Padova [b], Padova, Italy, Università di Trento [c], Trento, Italy

P. Azzi[a], N. Bacchetta[a], L. Benato[a,b], A. Boletti[a,b], R. Carlin[a,b], A. Carvalho Antunes De Oliveira[a,b], P. Checchia[a], M. Dall'Osso[a,b], P. De Castro Manzano[a], T. Dorigo[a], U. Dosselli[a], F. Gasparini[a,b], U. Gasparini[a,b], A. Gozzelino[a], S. Lacaprara[a], P. Lujan, A.T. Meneguzzo[a,b], M. Pegoraro[a], N. Pozzobon[a,b], P. Ronchese[a,b], R. Rossin[a,b], F. Simonetto[a,b], A. Tiko, E. Torassa[a], M. Zanetti[a,b], P. Zotto[a,b], G. Zumerle[a,b]

INFN Sezione di Pavia [a], Università di Pavia [b], Pavia, Italy

A. Braghieri[a], A. Magnani[a], P. Montagna[a,b], S.P. Ratti[a,b], V. Re[a], M. Ressegotti[a,b], C. Riccardi[a,b], P. Salvini[a], I. Vai[a,b], P. Vitulo[a,b]

INFN Sezione di Perugia [a], Università di Perugia [b], Perugia, Italy

L. Alunni Solestizi[a,b], M. Biasini[a,b], G.M. Bilei[a], C. Cecchi[a,b], D. Ciangottini[a,b], L. Fanò[a,b], P. Lariccia[a,b], R. Leonardi[a,b], E. Manoni[a], G. Mantovani[a,b], V. Mariani[a,b], M. Menichelli[a], A. Rossi[a,b], A. Santocchia[a,b], D. Spiga[a]

INFN Sezione di Pisa [a], Università di Pisa [b], Scuola Normale Superiore di Pisa [c], Pisa, Italy

K. Androsov[a], P. Azzurri[a,16], G. Bagliesi[a], L. Bianchini[a], T. Boccali[a], L. Borrello, R. Castaldi[a], M.A. Ciocci[a,b], R. Dell'Orso[a], G. Fedi[a], L. Giannini[a,c], A. Giassi[a], M.T. Grippo[a,31], F. Ligabue[a,c], T. Lomtadze[a], E. Manca[a,c], G. Mandorli[a,c], A. Messineo[a,b], F. Palla[a], A. Rizzi[a,b], P. Spagnolo[a], R. Tenchini[a], G. Tonelli[a,b], A. Venturi[a], P.G. Verdini[a]

JHEP08(2018)066

INFN Sezione di Roma [a], Sapienza Università di Roma [b], Rome, Italy
L. Barone[a,b], F. Cavallari[a], M. Cipriani[a,b], N. Daci[a], D. Del Re[a,b], E. Di Marco[a,b], M. Diemoz[a], S. Gelli[a,b], E. Longo[a,b], B. Marzocchi[a,b], P. Meridiani[a], G. Organtini[a,b], F. Pandolfi[a], R. Paramatti[a,b], F. Preiato[a,b], S. Rahatlou[a,b], C. Rovelli[a], F. Santanastasio[a,b]

INFN Sezione di Torino [a], Università di Torino [b], Torino, Italy, Università del Piemonte Orientale [c], Novara, Italy
N. Amapane[a,b], R. Arcidiacono[a,c], S. Argiro[a,b], M. Arneodo[a,c], N. Bartosik[a], R. Bellan[a,b], C. Biino[a], N. Cartiglia[a], R. Castello[a,b], F. Cenna[a,b], M. Costa[a,b], R. Covarelli[a,b], A. Degano[a,b], N. Demaria[a], B. Kiani[a,b], C. Mariotti[a], S. Maselli[a], E. Migliore[a,b], V. Monaco[a,b], E. Monteil[a,b], M. Monteno[a], M.M. Obertino[a,b], L. Pacher[a,b], N. Pastrone[a], M. Pelliccioni[a], G.L. Pinna Angioni[a,b], A. Romero[a,b], M. Ruspa[a,c], R. Sacchi[a,b], K. Shchelina[a,b], V. Sola[a], A. Solano[a,b], A. Staiano[a]

INFN Sezione di Trieste [a], Università di Trieste [b], Trieste, Italy
S. Belforte[a], M. Casarsa[a], F. Cossutti[a], G. Della Ricca[a,b], A. Zanetti[a]

Kyungpook National University
D.H. Kim, G.N. Kim, M.S. Kim, J. Lee, S. Lee, S.W. Lee, C.S. Moon, Y.D. Oh, S. Sekmen, D.C. Son, Y.C. Yang

Chonnam National University, Institute for Universe and Elementary Particles, Kwangju, Korea
H. Kim, D.H. Moon, G. Oh

Hanyang University, Seoul, Korea
J.A. Brochero Cifuentes, J. Goh, T.J. Kim

Korea University, Seoul, Korea
S. Cho, S. Choi, Y. Go, D. Gyun, S. Ha, B. Hong, Y. Jo, Y. Kim, K. Lee, K.S. Lee, S. Lee, J. Lim, S.K. Park, Y. Roh

Seoul National University, Seoul, Korea
J. Almond, J. Kim, J.S. Kim, H. Lee, K. Lee, K. Nam, S.B. Oh, B.C. Radburn-Smith, S.h. Seo, U.K. Yang, H.D. Yoo, G.B. Yu

University of Seoul, Seoul, Korea
H. Kim, J.H. Kim, J.S.H. Lee, I.C. Park

Sungkyunkwan University, Suwon, Korea
Y. Choi, C. Hwang, J. Lee, I. Yu

Vilnius University, Vilnius, Lithuania
V. Dudenas, A. Juodagalvis, J. Vaitkus

National Centre for Particle Physics, Universiti Malaya, Kuala Lumpur, Malaysia
I. Ahmed, Z.A. Ibrahim, M.A.B. Md Ali[33], F. Mohamad Idris[34], W.A.T. Wan Abdullah, M.N. Yusli, Z. Zolkapli

JHEP08(2018)066

Centro de Investigacion y de Estudios Avanzados del IPN, Mexico City, Mexico

M.C. Duran-Osuna, H. Castilla-Valdez, E. De La Cruz-Burelo, G. Ramirez-Sanchez, I. Heredia-De La Cruz[35], R.I. Rabadan-Trejo, R. Lopez-Fernandez, J. Mejia Guisao, R. Reyes-Almanza, A. Sanchez-Hernandez

Universidad Iberoamericana, Mexico City, Mexico

S. Carrillo Moreno, C. Oropeza Barrera, F. Vazquez Valencia

Benemerita Universidad Autonoma de Puebla, Puebla, Mexico

J. Eysermans, I. Pedraza, H.A. Salazar Ibarguen, C. Uribe Estrada

Universidad Autónoma de San Luis Potosí, San Luis Potosí, Mexico

A. Morelos Pineda

University of Auckland, Auckland, New Zealand

D. Krofcheck

University of Canterbury, Christchurch, New Zealand

S. Bheesette, P.H. Butler

National Centre for Physics, Quaid-I-Azam University, Islamabad, Pakistan

A. Ahmad, M. Ahmad, Q. Hassan, H.R. Hoorani, A. Saddique, M.A. Shah, M. Shoaib, M. Waqas

National Centre for Nuclear Research, Swierk, Poland

H. Bialkowska, M. Bluj, B. Boimska, T. Frueboes, M. Górski, M. Kazana, K. Nawrocki, M. Szleper, P. Traczyk, P. Zalewski

Institute of Experimental Physics, Faculty of Physics, University of Warsaw, Warsaw, Poland

K. Bunkowski, A. Byszuk[36], K. Doroba, A. Kalinowski, M. Konecki, J. Krolikowski, M. Misiura, M. Olszewski, A. Pyskir, M. Walczak

Laboratório de Instrumentação e Física Experimental de Partículas, Lisboa, Portugal

P. Bargassa, C. Beirão Da Cruz E Silva, A. Di Francesco, P. Faccioli, B. Galinhas, M. Gallinaro, J. Hollar, N. Leonardo, L. Lloret Iglesias, M.V. Nemallapudi, J. Seixas, G. Strong, O. Toldaiev, D. Vadruccio, J. Varela

Joint Institute for Nuclear Research, Dubna, Russia

S. Afanasiev, P. Bunin, M. Gavrilenko, I. Golutvin, I. Gorbunov, A. Kamenev, V. Karjavin, A. Lanev, A. Malakhov, V. Matveev[37,38], P. Moisenz, V. Palichik, V. Perelygin, S. Shmatov, S. Shulha, N. Skatchkov, V. Smirnov, N. Voytishin, A. Zarubin

Petersburg Nuclear Physics Institute, Gatchina (St. Petersburg), Russia

Y. Ivanov, V. Kim[39], E. Kuznetsova[40], P. Levchenko, V. Murzin, V. Oreshkin, I. Smirnov, D. Sosnov, V. Sulimov, L. Uvarov, S. Vavilov, A. Vorobyev

JHEP08(2018)066

Institute for Nuclear Research, Moscow, Russia

Yu. Andreev, A. Dermenev, S. Gninenko, N. Golubev, A. Karneyeu, M. Kirsanov, N. Krasnikov, A. Pashenkov, D. Tlisov, A. Toropin

Institute for Theoretical and Experimental Physics, Moscow, Russia

V. Epshteyn, V. Gavrilov, N. Lychkovskaya, V. Popov, I. Pozdnyakov, G. Safronov, A. Spiridonov, A. Stepennov, V. Stolin, M. Toms, E. Vlasov, A. Zhokin

Moscow Institute of Physics and Technology, Moscow, Russia

T. Aushev, A. Bylinkin[38]

National Research Nuclear University 'Moscow Engineering Physics Institute' (MEPhI), Moscow, Russia

M. Chadeeva[41], P. Parygin, D. Philippov, S. Polikarpov, E. Popova, V. Rusinov

P.N. Lebedev Physical Institute, Moscow, Russia

V. Andreev, M. Azarkin[38], I. Dremin[38], M. Kirakosyan[38], S.V. Rusakov, A. Terkulov

Skobeltsyn Institute of Nuclear Physics, Lomonosov Moscow State University, Moscow, Russia

A. Baskakov, A. Belyaev, E. Boos, V. Bunichev, M. Dubinin[42], L. Dudko, V. Klyukhin, O. Kodolova, N. Korneeva, I. Lokhtin, I. Miagkov, S. Obraztsov, M. Perfilov, S. Petrushanko, V. Savrin

Novosibirsk State University (NSU), Novosibirsk, Russia

V. Blinov[43], D. Shtol[43], Y. Skovpen[43]

State Research Center of Russian Federation, Institute for High Energy Physics of NRC &quot, Kurchatov Institute&quot, , Protvino, Russia

I. Azhgirey, I. Bayshev, S. Bitioukov, D. Elumakhov, A. Godizov, V. Kachanov, A. Kalinin, D. Konstantinov, P. Mandrik, V. Petrov, R. Ryutin, A. Sobol, S. Troshin, N. Tyurin, A. Uzunian, A. Volkov

National Research Tomsk Polytechnic University, Tomsk, Russia

A. Babaev

University of Belgrade, Faculty of Physics and Vinca Institute of Nuclear Sciences, Belgrade, Serbia

P. Adzic[44], P. Cirkovic, D. Devetak, M. Dordevic, J. Milosevic

Centro de Investigaciones Energéticas Medioambientales y Tecnológicas (CIEMAT), Madrid, Spain

J. Alcaraz Maestre, A. Álvarez Fernández, I. Bachiller, M. Barrio Luna, M. Cerrada, N. Colino, B. De La Cruz, A. Delgado Peris, C. Fernandez Bedoya, J.P. Fernández Ramos, J. Flix, M.C. Fouz, O. Gonzalez Lopez, S. Goy Lopez, J.M. Hernandez, M.I. Josa, D. Moran, A. Pérez-Calero Yzquierdo, J. Puerta Pelayo, I. Redondo, L. Romero, M.S. Soares, A. Triossi

JHEP08(2018)066

Universidad Autónoma de Madrid, Madrid, Spain

C. Albajar, J.F. de Trocóniz

Universidad de Oviedo, Oviedo, Spain

J. Cuevas, C. Erice, J. Fernandez Menendez, S. Folgueras, I. Gonzalez Caballero, J.R. González Fernández, E. Palencia Cortezon, S. Sanchez Cruz, P. Vischia, J.M. Vizan Garcia

Instituto de Física de Cantabria (IFCA), CSIC-Universidad de Cantabria, Santander, Spain

I.J. Cabrillo, A. Calderon, B. Chazin Quero, J. Duarte Campderros, M. Fernandez, P.J. Fernández Manteca, A. García Alonso, J. Garcia-Ferrero, G. Gomez, A. Lopez Virto, J. Marco, C. Martinez Rivero, P. Martinez Ruiz del Arbol, F. Matorras, J. Piedra Gomez, C. Prieels, T. Rodrigo, A. Ruiz-Jimeno, L. Scodellaro, N. Trevisani, I. Vila, R. Vilar Cortabitarte

CERN, European Organization for Nuclear Research, Geneva, Switzerland

D. Abbaneo, B. Akgun, E. Auffray, P. Baillon, A.H. Ball, D. Barney, J. Bendavid, M. Bianco, A. Bocci, C. Botta, T. Camporesi, M. Cepeda, G. Cerminara, E. Chapon, Y. Chen, D. d'Enterria, A. Dabrowski, V. Daponte, A. David, M. De Gruttola, A. De Roeck, N. Deelen, M. Dobson, T. du Pree, M. Dünser, N. Dupont, A. Elliott-Peisert, P. Everaerts, F. Fallavollita[45], G. Franzoni, J. Fulcher, W. Funk, D. Gigi, A. Gilbert, K. Gill, F. Glege, D. Gulhan, J. Hegeman, V. Innocente, A. Jafari, P. Janot, O. Karacheban[19], J. Kieseler, V. Knünz, A. Kornmayer, M. Krammer[1], C. Lange, P. Lecoq, C. Lourenço, M.T. Lucchini, L. Malgeri, M. Mannelli, A. Martelli, F. Meijers, J.A. Merlin, S. Mersi, E. Meschi, P. Milenovic[46], F. Moortgat, M. Mulders, H. Neugebauer, J. Ngadiuba, S. Orfanelli, L. Orsini, F. Pantaleo[16], L. Pape, E. Perez, M. Peruzzi, A. Petrilli, G. Petrucciani, A. Pfeiffer, M. Pierini, F.M. Pitters, D. Rabady, A. Racz, T. Reis, G. Rolandi[47], M. Rovere, H. Sakulin, C. Schäfer, C. Schwick, M. Seidel, M. Selvaggi, A. Sharma, P. Silva, P. Sphicas[48], A. Stakia, J. Steggemann, M. Stoye, M. Tosi, D. Treille, A. Tsirou, V. Veckalns[49], M. Verweij, W.D. Zeuner

Paul Scherrer Institut, Villigen, Switzerland

W. Bertl[†], L. Caminada[50], K. Deiters, W. Erdmann, R. Horisberger, Q. Ingram, H.C. Kaestli, D. Kotlinski, U. Langenegger, T. Rohe, S.A. Wiederkehr

ETH Zurich — Institute for Particle Physics and Astrophysics (IPA), Zurich, Switzerland

M. Backhaus, L. Bäni, P. Berger, B. Casal, N. Chernyavskaya, G. Dissertori, M. Dittmar, M. Donegà, C. Dorfer, C. Grab, C. Heidegger, D. Hits, J. Hoss, T. Klijnsma, W. Lustermann, M. Marionneau, M.T. Meinhard, D. Meister, F. Micheli, P. Musella, F. Nessi-Tedaldi, J. Pata, F. Pauss, G. Perrin, L. Perrozzi, M. Quittnat, M. Reichmann, D. Ruini, D.A. Sanz Becerra, M. Schönenberger, L. Shchutska, V.R. Tavolaro, K. Theofilatos, M.L. Vesterbacka Olsson, R. Wallny, D.H. Zhu

JHEP08(2018)066

Universität Zürich, Zurich, Switzerland

T.K. Aarrestad, C. Amsler[51], D. Brzhechko, M.F. Canelli, A. De Cosa, R. Del Burgo, S. Donato, C. Galloni, T. Hreus, B. Kilminster, I. Neutelings, D. Pinna, G. Rauco, P. Robmann, D. Salerno, K. Schweiger, C. Seitz, Y. Takahashi, A. Zucchetta

National Central University, Chung-Li, Taiwan

V. Candelise, Y.H. Chang, K.y. Cheng, T.H. Doan, Sh. Jain, R. Khurana, C.M. Kuo, W. Lin, A. Pozdnyakov, S.S. Yu

National Taiwan University (NTU), Taipei, Taiwan

P. Chang, Y. Chao, K.F. Chen, P.H. Chen, F. Fiori, W.-S. Hou, Y. Hsiung, Arun Kumar, Y.F. Liu, R.-S. Lu, E. Paganis, A. Psallidas, A. Steen, J.f. Tsai

Chulalongkorn University, Faculty of Science, Department of Physics, Bangkok, Thailand

B. Asavapibhop, K. Kovitanggoon, G. Singh, N. Srimanobhas

Çukurova University, Physics Department, Science and Art Faculty, Adana, Turkey

M.N. Bakirci[52], A. Bat, F. Boran, S. Cerci[53], S. Damarseckin, Z.S. Demiroglu, C. Dozen, I. Dumanoglu, S. Girgis, G. Gokbulut, Y. Guler, I. Hos[54], E.E. Kangal[55], O. Kara, A. Kayis Topaksu, U. Kiminsu, M. Oglakci, G. Onengut, K. Ozdemir[56], B. Tali[53], U.G. Tok, S. Turkcapar, I.S. Zorbakir, C. Zorbilmez

Middle East Technical University, Physics Department, Ankara, Turkey

G. Karapinar[57], K. Ocalan[58], M. Yalvac, M. Zeyrek

Bogazici University, Istanbul, Turkey

E. Gülmez, M. Kaya[59], O. Kaya[60], S. Tekten, E.A. Yetkin[61]

Istanbul Technical University, Istanbul, Turkey

M.N. Agaras, S. Atay, A. Cakir, K. Cankocak, Y. Komurcu

Institute for Scintillation Materials of National Academy of Science of Ukraine, Kharkov, Ukraine

B. Grynyov

National Scientific Center, Kharkov Institute of Physics and Technology, Kharkov, Ukraine

L. Levchuk

University of Bristol, Bristol, United Kingdom

F. Ball, L. Beck, J.J. Brooke, D. Burns, E. Clement, D. Cussans, O. Davignon, H. Flacher, J. Goldstein, G.P. Heath, H.F. Heath, L. Kreczko, D.M. Newbold[62], S. Paramesvaran, T. Sakuma, S. Seif El Nasr-storey, D. Smith, V.J. Smith

JHEP08(2018)066

Rutherford Appleton Laboratory, Didcot, United Kingdom
K.W. Bell, A. Belyaev[63], C. Brew, R.M. Brown, D. Cieri, D.J.A. Cockerill, J.A. Coughlan, K. Harder, S. Harper, J. Linacre, E. Olaiya, D. Petyt, C.H. Shepherd-Themistocleous, A. Thea, I.R. Tomalin, T. Williams, W.J. Womersley

Imperial College, London, United Kingdom
G. Auzinger, R. Bainbridge, P. Bloch, J. Borg, S. Breeze, O. Buchmuller, A. Bundock, S. Casasso, D. Colling, L. Corpe, P. Dauncey, G. Davies, M. Della Negra, R. Di Maria, A. Elwood, Y. Haddad, G. Hall, G. Iles, T. James, M. Komm, R. Lane, C. Laner, L. Lyons, A.-M. Magnan, S. Malik, L. Mastrolorenzo, T. Matsushita, J. Nash[64], A. Nikitenko[7], V. Palladino, M. Pesaresi, A. Richards, A. Rose, E. Scott, C. Seez, A. Shtipliyski, T. Strebler, S. Summers, A. Tapper, K. Uchida, M. Vazquez Acosta[65], T. Virdee[16], N. Wardle, D. Winterbottom, J. Wright, S.C. Zenz

Brunel University, Uxbridge, United Kingdom
J.E. Cole, P.R. Hobson, A. Khan, P. Kyberd, A. Morton, I.D. Reid, L. Teodorescu, S. Zahid

Baylor University, Waco, U.S.A.
A. Borzou, K. Call, J. Dittmann, K. Hatakeyama, H. Liu, N. Pastika, C. Smith

Catholic University of America, Washington DC, U.S.A.
R. Bartek, A. Dominguez

The University of Alabama, Tuscaloosa, U.S.A.
A. Buccilli, S.I. Cooper, C. Henderson, P. Rumerio, C. West

Boston University, Boston, U.S.A.
D. Arcaro, A. Avetisyan, T. Bose, D. Gastler, D. Rankin, C. Richardson, J. Rohlf, L. Sulak, D. Zou

Brown University, Providence, U.S.A.
G. Benelli, D. Cutts, M. Hadley, J. Hakala, U. Heintz, J.M. Hogan[66], K.H.M. Kwok, E. Laird, G. Landsberg, J. Lee, Z. Mao, M. Narain, J. Pazzini, S. Piperov, S. Sagir, R. Syarif, D. Yu

University of California, Davis, Davis, U.S.A.
R. Band, C. Brainerd, R. Breedon, D. Burns, M. Calderon De La Barca Sanchez, M. Chertok, J. Conway, R. Conway, P.T. Cox, R. Erbacher, C. Flores, G. Funk, W. Ko, R. Lander, C. Mclean, M. Mulhearn, D. Pellett, J. Pilot, S. Shalhout, M. Shi, J. Smith, D. Stolp, D. Taylor, K. Tos, M. Tripathi, Z. Wang, F. Zhang

University of California, Los Angeles, U.S.A.
M. Bachtis, C. Bravo, R. Cousins, A. Dasgupta, A. Florent, J. Hauser, M. Ignatenko, N. Mccoll, S. Regnard, D. Saltzberg, C. Schnaible, V. Valuev

University of California, Riverside, Riverside, U.S.A.
E. Bouvier, K. Burt, R. Clare, J. Ellison, J.W. Gary, S.M.A. Ghiasi Shirazi, G. Hanson, G. Karapostoli, E. Kennedy, F. Lacroix, O.R. Long, M. Olmedo Negrete, M.I. Paneva, W. Si, L. Wang, H. Wei, S. Wimpenny, B. R. Yates

JHEP08(2018)066

University of California, San Diego, La Jolla, U.S.A.

J.G. Branson, S. Cittolin, M. Derdzinski, R. Gerosa, D. Gilbert, B. Hashemi, A. Holzner, D. Klein, G. Kole, V. Krutelyov, J. Letts, M. Masciovecchio, D. Olivito, S. Padhi, M. Pieri, M. Sani, V. Sharma, S. Simon, M. Tadel, A. Vartak, S. Wasserbaech[67], J. Wood, F. Würthwein, A. Yagil, G. Zevi Della Porta

University of California, Santa Barbara — Department of Physics, Santa Barbara, U.S.A.

N. Amin, R. Bhandari, J. Bradmiller-Feld, C. Campagnari, M. Citron, A. Dishaw, V. Dutta, M. Franco Sevilla, L. Gouskos, R. Heller, J. Incandela, A. Ovcharova, H. Qu, J. Richman, D. Stuart, I. Suarez, J. Yoo

California Institute of Technology, Pasadena, U.S.A.

D. Anderson, A. Bornheim, J. Bunn, J.M. Lawhorn, H.B. Newman, T. Q. Nguyen, C. Pena, M. Spiropulu, J.R. Vlimant, R. Wilkinson, S. Xie, Z. Zhang, R.Y. Zhu

Carnegie Mellon University, Pittsburgh, U.S.A.

M.B. Andrews, T. Ferguson, T. Mudholkar, M. Paulini, J. Russ, M. Sun, H. Vogel, I. Vorobiev, M. Weinberg

University of Colorado Boulder, Boulder, U.S.A.

J.P. Cumalat, W.T. Ford, F. Jensen, A. Johnson, M. Krohn, S. Leontsinis, E. MacDonald, T. Mulholland, K. Stenson, K.A. Ulmer, S.R. Wagner

Cornell University, Ithaca, U.S.A.

J. Alexander, J. Chaves, Y. Cheng, J. Chu, A. Datta, K. Mcdermott, N. Mirman, J.R. Patterson, D. Quach, A. Rinkevicius, A. Ryd, L. Skinnari, L. Soffi, S.M. Tan, Z. Tao, J. Thom, J. Tucker, P. Wittich, M. Zientek

Fermi National Accelerator Laboratory, Batavia, U.S.A.

S. Abdullin, M. Albrow, M. Alyari, G. Apollinari, A. Apresyan, A. Apyan, S. Banerjee, L.A.T. Bauerdick, A. Beretvas, J. Berryhill, P.C. Bhat, G. Bolla[†], K. Burkett, J.N. Butler, A. Canepa, G.B. Cerati, H.W.K. Cheung, F. Chlebana, M. Cremonesi, J. Duarte, V.D. Elvira, J. Freeman, Z. Gecse, E. Gottschalk, L. Gray, D. Green, S. Grünendahl, O. Gutsche, J. Hanlon, R.M. Harris, S. Hasegawa, J. Hirschauer, Z. Hu, B. Jayatilaka, S. Jindariani, M. Johnson, U. Joshi, B. Klima, M.J. Kortelainen, B. Kreis, S. Lammel, D. Lincoln, R. Lipton, M. Liu, T. Liu, R. Lopes De Sá, J. Lykken, K. Maeshima, N. Magini, J.M. Marraffino, D. Mason, P. McBride, P. Merkel, S. Mrenna, S. Nahn, V. O'Dell, K. Pedro, O. Prokofyev, G. Rakness, L. Ristori, A. Savoy-Navarro[68], B. Schneider, E. Sexton-Kennedy, A. Soha, W.J. Spalding, L. Spiegel, S. Stoynev, J. Strait, N. Strobbe, L. Taylor, S. Tkaczyk, N.V. Tran, L. Uplegger, E.W. Vaandering, C. Vernieri, M. Verzocchi, R. Vidal, M. Wang, H.A. Weber, A. Whitbeck, W. Wu

University of Florida, Gainesville, U.S.A.

D. Acosta, P. Avery, P. Bortignon, D. Bourilkov, A. Brinkerhoff, A. Carnes, M. Carver, D. Curry, R.D. Field, I.K. Furic, S.V. Gleyzer, B.M. Joshi, J. Konigsberg, A. Korytov,

JHEP08(2018)066

K. Kotov, P. Ma, K. Matchev, H. Mei, G. Mitselmakher, K. Shi, D. Sperka, N. Terentyev, L. Thomas, J. Wang, S. Wang, J. Yelton

Florida International University, Miami, U.S.A.
Y.R. Joshi, S. Linn, P. Markowitz, J.L. Rodriguez

Florida State University, Tallahassee, U.S.A.
A. Ackert, T. Adams, A. Askew, S. Hagopian, V. Hagopian, K.F. Johnson, T. Kolberg, G. Martinez, T. Perry, H. Prosper, A. Saha, A. Santra, V. Sharma, R. Yohay

Florida Institute of Technology, Melbourne, U.S.A.
M.M. Baarmand, V. Bhopatkar, S. Colafranceschi, M. Hohlmann, D. Noonan, T. Roy, F. Yumiceva

University of Illinois at Chicago (UIC), Chicago, U.S.A.
M.R. Adams, L. Apanasevich, D. Berry, R.R. Betts, R. Cavanaugh, X. Chen, S. Dittmer, O. Evdokimov, C.E. Gerber, D.A. Hangal, D.J. Hofman, K. Jung, J. Kamin, I.D. Sandoval Gonzalez, M.B. Tonjes, N. Varelas, H. Wang, Z. Wu, J. Zhang

The University of Iowa, Iowa City, U.S.A.
B. Bilki[69], W. Clarida, K. Dilsiz[70], S. Durgut, R.P. Gandrajula, M. Haytmyradov, V. Khristenko, J.-P. Merlo, H. Mermerkaya[71], A. Mestvirishvili, A. Moeller, J. Nachtman, H. Ogul[72], Y. Onel, F. Ozok[73], A. Penzo, C. Snyder, E. Tiras, J. Wetzel, K. Yi

Johns Hopkins University, Baltimore, U.S.A.
B. Blumenfeld, A. Cocoros, N. Eminizer, D. Fehling, L. Feng, A.V. Gritsan, P. Maksimovic, J. Roskes, U. Sarica, M. Swartz, M. Xiao, C. You

The University of Kansas, Lawrence, U.S.A.
A. Al-bataineh, P. Baringer, A. Bean, S. Boren, J. Bowen, J. Castle, S. Khalil, A. Kropivnitskaya, D. Majumder, W. Mcbrayer, M. Murray, C. Rogan, C. Royon, S. Sanders, E. Schmitz, J.D. Tapia Takaki, Q. Wang

Kansas State University, Manhattan, U.S.A.
A. Ivanov, K. Kaadze, Y. Maravin, A. Modak, A. Mohammadi, L.K. Saini, N. Skhirtladze

Lawrence Livermore National Laboratory, Livermore, U.S.A.
F. Rebassoo, D. Wright

University of Maryland, College Park, U.S.A.
A. Baden, O. Baron, A. Belloni, S.C. Eno, Y. Feng, C. Ferraioli, N.J. Hadley, S. Jabeen, G.Y. Jeng, R.G. Kellogg, J. Kunkle, A.C. Mignerey, F. Ricci-Tam, Y.H. Shin, A. Skuja, S.C. Tonwar

Massachusetts Institute of Technology, Cambridge, U.S.A.
D. Abercrombie, B. Allen, V. Azzolini, R. Barbieri, A. Baty, G. Bauer, R. Bi, S. Brandt, W. Busza, I.A. Cali, M. D'Alfonso, Z. Demiragli, G. Gomez Ceballos, M. Goncharov, P. Harris, D. Hsu, M. Hu, Y. Iiyama, G.M. Innocenti, M. Klute, D. Kovalskyi, Y.-J. Lee, A. Levin, P.D. Luckey, B. Maier, A.C. Marini, C. Mcginn, C. Mironov, S. Narayanan,

JHEP08(2018)066

X. Niu, C. Paus, C. Roland, G. Roland, G.S.F. Stephans, K. Sumorok, K. Tatar, D. Velicanu, J. Wang, T.W. Wang, B. Wyslouch, S. Zhaozhong

University of Minnesota, Minneapolis, U.S.A.

A.C. Benvenuti, R.M. Chatterjee, A. Evans, P. Hansen, S. Kalafut, Y. Kubota, Z. Lesko, J. Mans, S. Nourbakhsh, N. Ruckstuhl, R. Rusack, J. Turkewitz, M.A. Wadud

University of Mississippi, Oxford, U.S.A.

J.G. Acosta, S. Oliveros

University of Nebraska-Lincoln, Lincoln, U.S.A.

E. Avdeeva, K. Bloom, D.R. Claes, C. Fangmeier, F. Golf, R. Gonzalez Suarez, R. Kamalieddin, I. Kravchenko, J. Monroy, J.E. Siado, G.R. Snow, B. Stieger

State University of New York at Buffalo, Buffalo, U.S.A.

A. Godshalk, C. Harrington, I. Iashvili, D. Nguyen, A. Parker, S. Rappoccio, B. Roozbahani

Northeastern University, Boston, U.S.A.

G. Alverson, E. Barberis, C. Freer, A. Hortiangtham, A. Massironi, D.M. Morse, T. Orimoto, R. Teixeira De Lima, T. Wamorkar, B. Wang, A. Wisecarver, D. Wood

Northwestern University, Evanston, U.S.A.

S. Bhattacharya, O. Charaf, K.A. Hahn, N. Mucia, N. Odell, M.H. Schmitt, K. Sung, M. Trovato, M. Velasco

University of Notre Dame, Notre Dame, U.S.A.

R. Bucci, N. Dev, M. Hildreth, K. Hurtado Anampa, C. Jessop, D.J. Karmgard, N. Kellams, K. Lannon, W. Li, N. Loukas, N. Marinelli, F. Meng, C. Mueller, Y. Musienko[37], M. Planer, A. Reinsvold, R. Ruchti, P. Siddireddy, G. Smith, S. Taroni, M. Wayne, A. Wightman, M. Wolf, A. Woodard

The Ohio State University, Columbus, U.S.A.

J. Alimena, L. Antonelli, B. Bylsma, L.S. Durkin, S. Flowers, B. Francis, A. Hart, C. Hill, W. Ji, T.Y. Ling, W. Luo, B.L. Winer, H.W. Wulsin

Princeton University, Princeton, U.S.A.

S. Cooperstein, O. Driga, P. Elmer, J. Hardenbrook, P. Hebda, S. Higginbotham, A. Kalogeropoulos, D. Lange, J. Luo, D. Marlow, K. Mei, I. Ojalvo, J. Olsen, C. Palmer, P. Piroué, J. Salfeld-Nebgen, D. Stickland, C. Tully

University of Puerto Rico, Mayaguez, U.S.A.

S. Malik, S. Norberg

Purdue University, West Lafayette, U.S.A.

A. Barker, V.E. Barnes, S. Das, L. Gutay, M. Jones, A.W. Jung, A. Khatiwada, D.H. Miller, N. Neumeister, C.C. Peng, H. Qiu, J.F. Schulte, J. Sun, F. Wang, R. Xiao, W. Xie

Purdue University Northwest, Hammond, U.S.A.

T. Cheng, J. Dolen, N. Parashar

JHEP08(2018)066

Rice University, Houston, U.S.A.

Z. Chen, K.M. Ecklund, S. Freed, F.J.M. Geurts, M. Guilbaud, M. Kilpatrick, W. Li, B. Michlin, B.P. Padley, J. Roberts, J. Rorie, W. Shi, Z. Tu, J. Zabel, A. Zhang

University of Rochester, Rochester, U.S.A.

A. Bodek, P. de Barbaro, R. Demina, Y.t. Duh, T. Ferbel, M. Galanti, A. Garcia-Bellido, J. Han, O. Hindrichs, A. Khukhunaishvili, K.H. Lo, P. Tan, M. Verzetti

The Rockefeller University, New York, U.S.A.

R. Ciesielski, K. Goulianos, C. Mesropian

Rutgers, The State University of New Jersey, Piscataway, U.S.A.

A. Agapitos, J.P. Chou, Y. Gershtein, T.A. Gómez Espinosa, E. Halkiadakis, M. Heindl, E. Hughes, S. Kaplan, R. Kunnawalkam Elayavalli, S. Kyriacou, A. Lath, R. Montalvo, K. Nash, M. Osherson, H. Saka, S. Salur, S. Schnetzer, D. Sheffield, S. Somalwar, R. Stone, S. Thomas, P. Thomassen, M. Walker

University of Tennessee, Knoxville, U.S.A.

A.G. Delannoy, J. Heideman, G. Riley, K. Rose, S. Spanier, K. Thapa

Texas A&M University, College Station, U.S.A.

O. Bouhali[74], A. Castaneda Hernandez[74], A. Celik, M. Dalchenko, M. De Mattia, A. Delgado, S. Dildick, R. Eusebi, J. Gilmore, T. Huang, T. Kamon[75], R. Mueller, Y. Pakhotin, R. Patel, A. Perloff, L. Perniè, D. Rathjens, A. Safonov, A. Tatarinov

Texas Tech University, Lubbock, U.S.A.

N. Akchurin, J. Damgov, F. De Guio, P.R. Dudero, J. Faulkner, E. Gurpinar, S. Kunori, K. Lamichhane, S.W. Lee, T. Mengke, S. Muthumuni, T. Peltola, S. Undleeb, I. Volobouev, Z. Wang

Vanderbilt University, Nashville, U.S.A.

S. Greene, A. Gurrola, R. Janjam, W. Johns, C. Maguire, A. Melo, H. Ni, K. Padeken, J.D. Ruiz Alvarez, P. Sheldon, S. Tuo, J. Velkovska, Q. Xu

University of Virginia, Charlottesville, U.S.A.

M.W. Arenton, P. Barria, B. Cox, R. Hirosky, M. Joyce, A. Ledovskoy, H. Li, C. Neu, T. Sinthuprasith, Y. Wang, E. Wolfe, F. Xia

Wayne State University, Detroit, U.S.A.

R. Harr, P.E. Karchin, N. Poudyal, J. Sturdy, P. Thapa, S. Zaleski

University of Wisconsin — Madison, Madison, WI, U.S.A.

M. Brodski, J. Buchanan, C. Caillol, D. Carlsmith, S. Dasu, L. Dodd, S. Duric, B. Gomber, M. Grothe, M. Herndon, A. Hervé, U. Hussain, P. Klabbers, A. Lanaro, A. Levine, K. Long, R. Loveless, V. Rekovic, T. Ruggles, A. Savin, N. Smith, W.H. Smith, N. Woods

JHEP08(2018)066

†: Deceased
1: Also at Vienna University of Technology, Vienna, Austria
2: Also at IRFU; CEA; Université Paris-Saclay, Gif-sur-Yvette, France
3: Also at Universidade Estadual de Campinas, Campinas, Brazil
4: Also at Federal University of Rio Grande do Sul, Porto Alegre, Brazil
5: Also at Universidade Federal de Pelotas, Pelotas, Brazil
6: Also at Université Libre de Bruxelles, Bruxelles, Belgium
7: Also at Institute for Theoretical and Experimental Physics, Moscow, Russia
8: Also at Joint Institute for Nuclear Research, Dubna, Russia
9: Also at Cairo University, Cairo, Egypt
10: Also at Suez University, Suez, Egypt
11: Now at British University in Egypt, Cairo, Egypt
12: Also at Zewail City of Science and Technology, Zewail, Egypt
13: Also at Department of Physics; King Abdulaziz University, Jeddah, Saudi Arabia
14: Also at Université de Haute Alsace, Mulhouse, France
15: Also at Skobeltsyn Institute of Nuclear Physics; Lomonosov Moscow State University, Moscow, Russia
16: Also at CERN; European Organization for Nuclear Research, Geneva, Switzerland
17: Also at RWTH Aachen University; III. Physikalisches Institut A, Aachen, Germany
18: Also at University of Hamburg, Hamburg, Germany
19: Also at Brandenburg University of Technology, Cottbus, Germany
20: Also at MTA-ELTE Lendület CMS Particle and Nuclear Physics Group; Eötvös Loránd University, Budapest, Hungary
21: Also at Institute of Nuclear Research ATOMKI, Debrecen, Hungary
22: Also at Institute of Physics; University of Debrecen, Debrecen, Hungary
23: Also at Indian Institute of Technology Bhubaneswar, Bhubaneswar, India
24: Also at Institute of Physics, Bhubaneswar, India
25: Also at Shoolini University, Solan, India
26: Also at University of Visva-Bharati, Santiniketan, India
27: Also at University of Ruhuna, Matara, Sri Lanka
28: Also at Isfahan University of Technology, Isfahan, Iran
29: Also at Yazd University, Yazd, Iran
30: Also at Plasma Physics Research Center; Science and Research Branch; Islamic Azad University, Tehran, Iran
31: Also at Università degli Studi di Siena, Siena, Italy
32: Also at INFN Sezione di Milano-Bicocca; Università di Milano-Bicocca, Milano, Italy
33: Also at International Islamic University of Malaysia, Kuala Lumpur, Malaysia
34: Also at Malaysian Nuclear Agency; MOSTI, Kajang, Malaysia
35: Also at Consejo Nacional de Ciencia y Tecnología, Mexico city, Mexico
36: Also at Warsaw University of Technology; Institute of Electronic Systems, Warsaw, Poland
37: Also at Institute for Nuclear Research, Moscow, Russia
38: Now at National Research Nuclear University 'Moscow Engineering Physics Institute' (MEPhI), Moscow, Russia
39: Also at St. Petersburg State Polytechnical University, St. Petersburg, Russia
40: Also at University of Florida, Gainesville, U.S.A.
41: Also at P.N. Lebedev Physical Institute, Moscow, Russia
42: Also at California Institute of Technology, Pasadena, U.S.A.

JHEP08(2018)066

43: Also at Budker Institute of Nuclear Physics, Novosibirsk, Russia
44: Also at Faculty of Physics; University of Belgrade, Belgrade, Serbia
45: Also at INFN Sezione di Pavia; Università di Pavia, Pavia, Italy
46: Also at University of Belgrade; Faculty of Physics and Vinca Institute of Nuclear Sciences, Belgrade, Serbia
47: Also at Scuola Normale e Sezione dell'INFN, Pisa, Italy
48: Also at National and Kapodistrian University of Athens, Athens, Greece
49: Also at Riga Technical University, Riga, Latvia
50: Also at Universität Zürich, Zurich, Switzerland
51: Also at Stefan Meyer Institute for Subatomic Physics (SMI), Vienna, Austria
52: Also at Gaziosmanpasa University, Tokat, Turkey
53: Also at Adiyaman University, Adiyaman, Turkey
54: Also at Istanbul Aydin University, Istanbul, Turkey
55: Also at Mersin University, Mersin, Turkey
56: Also at Piri Reis University, Istanbul, Turkey
57: Also at Izmir Institute of Technology, Izmir, Turkey
58: Also at Necmettin Erbakan University, Konya, Turkey
59: Also at Marmara University, Istanbul, Turkey
60: Also at Kafkas University, Kars, Turkey
61: Also at Istanbul Bilgi University, Istanbul, Turkey
62: Also at Rutherford Appleton Laboratory, Didcot, United Kingdom
63: Also at School of Physics and Astronomy; University of Southampton, Southampton, United Kingdom
64: Also at Monash University; Faculty of Science, Clayton, Australia
65: Also at Instituto de Astrofísica de Canarias, La Laguna, Spain
66: Also at Bethel University, ST. PAUL, U.S.A.
67: Also at Utah Valley University, Orem, U.S.A.
68: Also at Purdue University, West Lafayette, U.S.A.
69: Also at Beykent University, Istanbul, Turkey
70: Also at Bingol University, Bingol, Turkey
71: Also at Erzincan University, Erzincan, Turkey
72: Also at Sinop University, Sinop, Turkey
73: Also at Mimar Sinan University; Istanbul, Istanbul, Turkey
74: Also at Texas A&M University at Qatar, Doha, Qatar
75: Also at Kyungpook National University, Daegu, Korea

JHEP08(2018)066